JACC: BASIC TO TRANSLATIONAL SCIENCE VOL. 8, NO. 10, 2023


ORIGINAL RESEARCH - PRECLINICAL

# Decreased FAM13B Expression Increases Atrial Fibrillation Susceptibility by Regulating Sodium Current and Calcium Handling

Gregory Tchou, PhD,[a,*] Daniela Ponce-Balbuena, PhD,[b,*] Nana Liu, MD, PhD,[a,*] Shamone Gore-Panter, PhD,[a,*] Jeffrey Hsu, PhD,[a,*,†] Fang Liu, PhD,[a,*,‡] Emmanuel Opoku, MS,[a] Gregory Brubaker, MS,[a] Sarah M. Schumacher, PhD,[a] Christine S. Moravec, PhD,[a,c] John Barnard, PhD,[d] David R. Van Wagoner, PhD,[a,c] Mina K. Chung, MD,[a,c] Jonathan D. Smith, PhD[a,c]

## VISUAL ABSTRACT

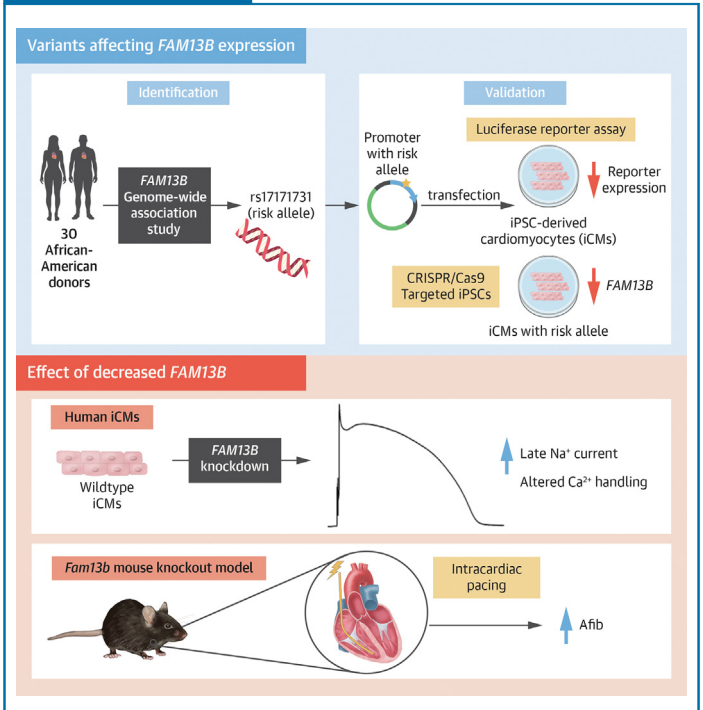


Tchou G, et al. J Am Coll Cardiol Basic Trans Science. 2023;8(10):1357–1378.

## HIGHLIGHTS

- **The risk allele of the AF-associated SNP rs17171731 has lower enhancer activity, binds to a second nuclear protein, and causes decreased *FAM13B* expression.**
- **Decreasing *FAM13B* expression in human stem cell–derived cardiomyocytes alters gene expression, increases the late/peak sodium current ratio, and alters the calcium transient.**
- ***Fam13b* KO mice have increased P-wave duration and QT interval and increased susceptibility to pacing-induced atrial and ventricular arrhythmias.**
- **The identification of the causal variant and responsible gene for the chromosome 5q31 AF susceptibility locus shows that FAM13B expression, its regulation, and downstream effects are targets for further investigation into disease mechanisms and patient-specific therapeutics.**

From the [a]Departments of Cardiovascular and Metabolic Sciences, Cleveland Clinic, Cleveland, Ohio, USA; [b]Department of Physiology and Cell Biology, Ohio State University, Columbus, Ohio, USA; [c]Department of Cardiovascular Medicine, Cleveland Clinic, Cleveland, Ohio, USA; and the [d]Department of Quantitative Health Sciences, Cleveland Clinic, Cleveland, Ohio, USA. *Drs Tchou and Ponce-Balbuena contributed equally to this work. †The current address of Dr Hsu is Ivy Natal, San Francisco, California, USA. ‡The current address of Dr Liu is Guilin Medical University, Guilin, Guangxi, China.

The authors attest they are in compliance with human studies committees and animal welfare regulations of the authors' institutions and Food and Drug Administration guidelines, including patient consent where appropriate. For more information, visit the Author Center.

Manuscript received January 23, 2023; revised manuscript received May 16, 2023, accepted May 16, 2023.

ISSN 2452-302X https://doi.org/10.1016/j.jacbts.2023.05.009

JACC: BASIC TO TRANSLATIONAL SCIENCE VOL. 8, NO. 10, 2023
OCTOBER 2023:1357–1378

## ABBREVIATIONS AND ACRONYMS

**6xHis** = 6 histidine
**AF** = atrial fibrillation
**ANOVA** = analysis of variance
**chr** = chromosome
**bp** = base pair
**ECG** = electrocardiogram
**eGFP** = enhanced green fluorescent protein
**eQTL** = expression quantitative trait loci
**FDR** = false discovery rate
**GFP** = green fluorescent protein
**GWAS** = genome-wide association study
**HDR** = homology-directed repair
**iCM** = stem cell–derived cardiomyocytes
**$I_{Na}$** = sodium current
**$I_{NaL}$** = late sodium current
**IRB** = institutional review board
**IsoP** = isoproterenol
**KD** = knockdown
**KO** = knockout
**LA** = left atrium
**LAA** = left atrial appendage
**LD** = linkage disequilibrium
**MBP** = maltose binding protein
**mRNA** = messenger RNA
**PPIA** = primer-limited cyclophilin A
**qRT-PCR** = quantitative reverse transcriptase-polymerase chain reaction
**rhFAM13B** = recombinant human FAM13B
**RhoGAP** = Rho GTPase-activating protein
**RNAseq** = next generation RNA sequencing
**Scr** = scrambled siRNA
**sgRNA** = single guide RNA
**siRNA** = small interfering RNA
**SNP** = single-nucleotide polymorphism
**WT** = wild type

## SUMMARY

A specific genetic variant associated with atrial fibrillation risk, rs17171731, was identified as a regulatory variant responsible for controlling *FAM13B* expression. The atrial fibrillation risk allele decreases *FAM13B* expression, whose knockdown alters the expression of many genes in stem cell–derived cardiomyocytes, including *SCN2B*, and led to pro-arrhythmogenic changes in the late sodium current and $Ca^{2+}$ cycling. *Fam13b* knockout mice had increased P-wave and QT interval duration and were more susceptible to pacing-induced arrhythmias vs control mice. *FAM13B* expression, its regulation, and downstream effects are potential targets for investigation of patient-specific therapeutics. (J Am Coll Cardiol Basic Trans Science 2023;8:1357–1378) 

Atrial fibrillation (AF) is the most common type of human arrhythmia and has a strong heritable component.[1] Recent genome-wide association studies (GWAS) for AF susceptibility identified ~140 loci associated with AF[2,3]; however, further functional genomic and cell biology studies for each GWAS locus are necessary to identify the causal gene, the causal genetic variant, and the mechanism for association with AF. Population studies reveal that most of the genetic risk for AF is not mendelian, but instead polygenic.[4] The polygenic component is made up of thousands to millions of effect-size weighted common single-nucleotide polymorphisms (SNPs), the vast majority with diminishingly small effect size, and a few with small to modest effect size. The vast majority of these common variants are not themselves, or are not in linkage disequilibrium (LD) with, variants that alter the protein amino acid sequence. Thus, we hypothesized that most of these GWAS loci are regulatory, leading to changes in gene expression rather than protein structure. As our prior left atrial appendage (LAA) next generation RNA sequencing (RNAseq) study showed, the expression levels of approximately two-thirds of all of the genes expressed in the LAA are associated with nearby common genetic variants, called *cis* expression quantitative trait loci (eQTLs).[5] We also identified the *cis* genes whose expression levels are associated with the top SNP at many AF GWAS loci.[5] We identified *FAM13B* as the gene whose expression is associated with the top GWAS SNP at chromosome (chr) 5q31, with the risk allele associated with decreased expression. Here, we describe how an eQTL analysis in a small African ancestry cohort led to the identification of a candidate causal SNP for the chr 5q31 GWAS locus, rs17171731, responsible for the regulation of *FAM13B* gene expression. We validated this candidate SNP through reporter gene transfections, gel mobility shift assays, and gene editing in human pluripotent stem cells. Thus, the chr 5q31 GWAS locus appears to be mediated by regulating the expression of *FAM13B*, a poorly characterized member of the Rho GTPase-activating protein (RhoGAP) gene family.[6,7] Although we failed to detect RhoGAP activity of recombinant FAM13B protein, our study shows that the FAM13B protein plays a role in cardiomyocyte physiology and provides in vivo evidence that the *FAM13B* gene is responsible for the AF susceptibility locus on chr 5q31 via arrhythmogenic, non-RhoGAP, mechanisms.

## METHODS

**DATA AND MATERIALS ACCESS.** LAA variance normalized RNAseq gene expression levels for each subject are available in the GEO database, accession number GSE69890. Human LAA eQTL data can be obtained on our web browser.[8] Custom scripts for eQTL analyses are also available.[9] RNAseq data from iCell cardiomyocyte FAM13B small interfering RNA (siRNA) vs scrambled siRNA treatment are available in the GEO database, accession number GSE221262. Other source files and data have been deposited in the Dryad accession number.[10]

**HUMAN LEFT ATRIAL TISSUE SAMPLES AND PROCESSING.** Human LAA tissues were obtained from patients undergoing elective surgery to treat AF, valve disease, or other cardiac disorders. LAA tissue specimens were also obtained from nonfailing donor hearts not used for transplantation. Demographic information for this population was previously published, and the 265 subjects included 235 subjects of European descent and 30 African descent or admixed subjects, with ancestry verified by SNP principal component

analysis.[5] Total RNA was isolated from LAA as described.[5] All surgical patients provided informed consent for research use of discarded atrial tissue. Before 2008, verbal consent was obtained and documented in the medical records in a process approved by the Cleveland Clinic Institutional Review Board (IRB). From 2008 onward, patients provided separate IRB-approved written informed consent. Tissue was also obtained from donor hearts not used for transplantation with written consent for research use provided by the family. The IRB approved the studies included in this report.

**GENOMIC DNA ISOLATION AND SNP MICROARRAY.** Genomic DNA from LAA tissue was genotyped using Illumina Hap550v3 and Hap610-quad SNP microarrays, as previously described.[5] To derive genotypes in addition to those on the microarray, the SNP data were imputed to 1000 Genomes Project phase 2 to generate genotypes for ~19 million SNPs, using the IMPUTE software.[11]

**ATRIAL RNA SEQUENCING AND ANALYSIS.** LAA RNA was isolated from the homogenate following the TRIzol protocol (Invitrogen). Library generation for RNAseq was done at the University of Chicago Genomics Facility using standard Illumina protocols (Part # 15015050, Rev A). As previously described,[5] 100-base pair (bp) paired-end sequencing was performed on the Illumina HiSeq 2000 platform and multiplexed to 6 samples across 2 lanes. Sequence reads were mapped to the human genome to derive a digital count of the expression of genes, which were defined using the Ensembl gene catalog (version 71). Reads were quantile normalized, and gene counts for eQTL analysis were variance-stabilized transformed as previously described.[5] eQTL analyses were performed separately for each racial group with beta-coefficients calculated as the additive effect of 1 allelic difference on $\log_2$ gene expression. Genetic multidimensional scaling from SNP array genotyping was additionally calculated and added as covariates for the eQTL calculation. matrixeQTL[12] was used to test associations between genotype and variance-stabilized counts. The qvalue package was used to calculate false discovery rate (FDR) from the complete list of *P* values.[13] DNAse I hypersensitivity in human fetal heart tissue over the FAM13B gene region was downloaded from the Roadmap Epigenomics Project.

**ANALYSIS OF FAM13B EXPRESSION FROM SINGLE-NUCLEI RNAseq DATA.** Normalized single-nuclei gene counts from 12 left atrial (LA) samples (2 replicates each from 6 individual donors) as provided by Tucker et al[14] were integrated using the anchor approach in Seurat.[15] Specifically, normalized data were scaled per experiment (LA replicate by unique donor); the 2,000 most variable genes from the scaled data were used to find integration anchor points in a 30-dimensional space; and then integrated to create a dataset with reduced batch variation.[16] The top 30 principal components from the integrated and rescaled dataset were used to construct a 2-dimensional UMAP plot with cell type labels per nuclei provided by Tucker et al.[14] Percentage of nuclei expressing *FAM13B* (gene count >0) was calculated pooling the 2 replicates per individual to produce 6 percentages per annotated cell type. Similarly, *FAM13B* gene expression counts per million were calculated per donor by summing the unnormalized nuclei counts per cell type per donor then calculating counts per million using the edgeR R package.[17]

**HUMAN STEM CELL CULTURE AND CARDIAC DIFFERENTIATION.** Human pluripotent stem cells (WiCell, catalog #WAO9) were cultured in mTeSR Plus media (STEMCELL Technologies) on plates coated with growth factor-reduced Matrigel (Corning, Cat#354230). After passaging, stem cells were cultured in the presence of 10 μM Y-27632 (Abcam, Cat#ab120129) for 1 day. Cardiac differentiation of stem cells was conducted using the STEMdiff Cardiomyocyte Differentiation Kit (STEMCELL Technologies, Cat#100-0215). Stem cell-derived cardiomyocytes (iCMs) typically demonstrated spontaneous beating 12 days after initiation of differentiation and were generally used 2 to 3 weeks post-differentiation.

**REPORTER GENE EXPRESSION ANALYSIS.** Twenty-six-mer oligonucleotides (Supplemental Table 1) containing the *FAM13B* SNP rs17171731 reference or risk allele sequences were cloned into the luciferase reporter pT81luc.[18] The luciferase reporter and the β-galactosidase expression vector pCH110 were transfected into iCMs via electroporation (Nucleofector-II program A-23, Lonza, Cat#VPH-5012). Cell lysates were prepared and analyzed for β-galactosidase and luciferase activities using the Dual Light Reporter Gene Assay system (ThermoFisher, Cat#T1003).

**FAM13B ELECTROPHORETIC MOBILITY SHIFT ASSAYS.** Twenty-six-mer oligonucleotides containing the rs17171731 reference or risk allele sequences (Supplemental Table 1) were labeled with γ-$^{32}$P-ATP (10 μCi/μL) using T4 polynucleotide kinase (NEB, Cat#M0201) and annealed with complementary oligonucleotides in 10 mM Tris, 1 mM EDTA, 50 mM NaCl. The resulting probes were combined on ice with human heart nuclear extract (Active Motif,

Cat#36041), 1.25 μg poly(dI dC) (Sigma-Aldrich, Cat#P4929), and reaction buffer (final concentration 45 mM KCl, 1 mM $MgCl_2$, 15 mM HEPES pH 7.9, 1 mM DTT, 3% Ficoll 400) in the presence or absence of unlabeled competitor oligonucleotides, then incubated at room temperature for 25 minutes before running on Novex 6% DNA Retardation gels (ThermoFisher, Cat#EC63655BOX). Dried Gels were exposed to X-ray film. We attempted to identify proteins bound to the probes by adding 0.5 to 1.0 μg of the following antibodies to the heart extract before incubating with the labeled probes: ABI3, ATF4, MTF-1, POU2F1, POU2F2, SOX4, and SOX8 (One World Lab).

**iCell CARDIOMYOCYTE CULTURE AND siRNA KNOCKDOWN OF *FAM13B*.** iCell cardiomyocytes (Cellular Dynamics, Cat#R1007) derived from human inducible pluripotent stem cells were cultured and siRNA knockdown (KD) was performed using Cellular Dynamics International protocols. In short, $1.5 \times 10^5$ iCell cardiomyocytes were plated per well in fibronectin (Sigma)-coated 12-well plates. The cells were cultured in iCell cardiomyocyte maintenance media (Cellular Dynamics, Cat#M1003) for 7 days; beating was usually observed by day 3. Final concentrations of 50 nM/well of control scrambled (Scr) siRNA (ThermoFisher/Ambion silencer select, Cat#4390843) or *FAM13B* siRNA (ThermoFisher/Ambion, Cat# 439242, id S27906) were transfected into iCell cardiomyocytes using the TransIT-TKO transfection reagent (Mirus Bio, Cat#MIR2150). The cells were incubated with the siRNA-reagent complexes for 48 to 96 hours followed by either cellular electrophysiology studies or total RNA isolation with TRIzol (ThermoFisher, Cat#15596018) extraction and purification using the RNeasy Micro Kit (Qiagen, Cat#74004).

**iCell RNAseq AND ANALYSIS.** One-hundred-bp paired-end sequencing was performed on the Illumina HiSeq 2000. The sequence reads were mapped to the human genome using the STAR aligner (version 2.3.0) to derive a digital count of the expression of genes, which were defined using the Ensembl gene catalog (version 69). Genes were filtered to ensure a counts per million >5 in at least 2 samples, resulting in 11,017 genes. Differential expression analyses of *FAM13B* siRNA-treated vs control Scr siRNA iCells was performed using the limma-voom approach[19] with FDR control. Ingenuity Pathway Analysis (version 76765844) was performed to identify the top canonical pathways and empirical networks. Gene set enrichment analysis was performed to test the self-contained null hypothesis for each geneset in the Kyoto Encyclopedia of Genes and Genomes, Reactome, Biocarta, and Hallmark geneset collections of the Molecular Signature Database version 7.5.1. using the fast approximation to the ROAST gene set test (FRY).[20] FRY uses an approximate rotation-based approach for assessing significance, which is well calibrated with small expression studies and performant across many gene sets.

**QUANTITATIVE REVERSE TRANSCRIPTASE-POLYMERASE CHAIN REACTION.** Total RNA from LAA or iCell cardiomyocytes was reverse transcribed into complementary DNA using SuperScript IV VILO Master Mix (ThermoFisher, Cat#11756050). TaqMan gene expression master mix (ThermoFisher, Cat#4369016), FAM13B primer/probe mix (Hs00991421_m1, ThermoFisher), and either primer-limited cardiac actin (ACTC1) primer/probe mix (Hs00606316_m1, ThermoFisher) or primer-limited cyclophilin A (PPIA) primer/probe mix (Hs04194521_s1, ThermoFisher) were combined for quantitative reverse transcriptase-polymerase chain reaction (qRT-PCR) samples. qRT-PCR was performed using a Bio-Rad CFX thermocycler calibrated for FAM and VIC fluorescent probes. Thermal cycling was performed with a hot-start at 95°C for 10 minutes, followed by 40 cycles of 95°C for 15 seconds and 60°C for 60 seconds. The $\Delta C_t$ values for FAM13B expression levels were calculated relative to ACTC1 or PPIA. $\Delta\Delta C_t$ values were used to calculate the decrease of FAM13B expression relative to control conditions and the results were converted to base 10 values by calculating $2^{-\Delta\Delta Ct}$.

**GENE EDITING OF RS17171731.** The rs17171731 SNP was targeted for indel mutation via CRISPR-Cas9-mediated nonhomologous end joining. Constitutive expression of Cas9 was introduced into pluripotent stem cells homozygous for the rs17171731 reference allele through stable transfection with pSpCas9(BB)-2A-Puro (PX459) v2.0 (Addgene, Cat#62988) and subsequent selection in puromycin. The resulting $Cas9^+$ stem cells were transfected via electroporation (Lonza, Cat#VPH-5012, Nucleofector program B-016) with a single guide RNA (sgRNA) targeting rs17171731 (Supplemental Table 2). The rs17171731 region in genomic DNA from clonally derived cell lines was amplified by PCR and subjected to next generation sequencing using the MiSeq platform (Illumina) in order to identify indel alleles (primers in Supplemental Table 2). A CRISPR-Cas9 homology-directed repair (HDR) selection strategy, similar to one we previously reported in mouse stem cells,[21] was then used to generate a stem cell line homozygous for the rs17171731 risk allele. Stem cells were stably transfected with a green fluorescent protein (GFP) plasmid (VectorBuilder, Cat#VB180718-

1085dmd) carrying 2 nonsense mutations (Supplemental Table 2), then transfected with sgRNAs targeting GFP and rs17171731, as well as single-stranded donor oligonucleotides to create edits leading to a functional GFP and the rs171717131 risk allele, respectively (Supplemental Table 2). GFP-positive, HDR-competent cells were isolated via flow cytometry, plated individually into 96-well plates coated with mitomycin C–inactivated mouse embryonic fibroblasts, and expanded clonally. Forty-eight colonies were analyzed via PCR product sequencing and the ICE v2 CRISPR Analysis Tool (Synthego) to identify cell lines carrying rs17171731 allele switches.[22] Wild-type (WT), complex insertion, and homozygous risk allele stem cells were differentiated into iCMs and FAM13B messenger RNA (mRNA) levels, normalized to PPIA, were measured by qRT-PCR as described previously.

**CELLULAR ELECTROPHYSIOLOGY.** Patch clamp studies of *FAM13B* KD cells focused on measurement of sodium currents ($I_{Na}$) in Scr and *FAM13B*-siRNA-treated iCell cardiomyocytes. Cells were replated at low density 24 hours after siRNA treatment to yield isolated cells, and electrophysiology studies were performed 48 to 96 hours after transfection. Sodium currents were recorded at room temperature using whole cell clamp techniques. Pipettes (Corning 8161 thin-walled glass, 1.5-3.0 MΩ, Warner Instruments, Cat#64-0816) were filled with a solution containing 135 mM CsCl2, 10 mM NaCl, 2 mM $CaCl_2$, 5 mM EGTA, 10 mM HEPES, 5 mM MgATP, and titrated to pH 7.2 with CsOH. The cells were continuously superfused with an extracellular solution containing 50 mM NaCl, 1.8 mM $CaCl_2$, 1 mM $MgCl_2$, 110 mM CsCl, 10 mM glucose, 10 mM HEPES, 1 μM nifedipine (added fresh daily), pH 7.4. Currents were recorded with an Axopatch 1C amplifier controlled with pClamp 8.1 software (Molecular Devices). After seal formation and patch rupture, whole cell access resistance was 2 to 5 MΩ. To maintain cell viability, resting potential was held at −60 mV, with more negative steps given 100 ms before depolarizing steps used to record sodium currents. Current amplitudes recorded with the steady-state inactivation protocol were fit with a Boltzmann curve in Clampfit 8.1 (pClamp, Molecular Devices). To avoid time-dependent changes in siRNA exposure, data were obtained from similar numbers of Scr and *FAM13B* siRNA-treated cells on each day.

**CALCIUM TRANSIENT ASSAY.** Intracellular $Ca^{2+}$ transients were measured using the IonOptix Contractility and Calcium system and protocols. iCell cardiomyocytes were plated at least 7 days before the experiment, allowing the cells to settle and spread on the glass coverslips. The assay was done 72 hours after *FAM13B* or Scr siRNAs transfection. On the experimental day, iCell cardiomyocytes were incubated with Fura-2 AM (100 μM) for 15 minutes at 37°C. The cells were then washed twice for 5 minutes with Tyrodes solution (134 mM NaCl, 12 mM NaHCO3, 2.9 mM KCl, 0.34 mM Na2HPO4, 1 mM MgCl2, 10 mM HEPES pH 7.4, 1.2 mM CaCl2, 10 mM glucose). The glass coverslips with cells were mounted to the perfusion chamber. Using the ×40 objective lens, the cells were identified and used for recording calcium transients. The cardiomyocytes were centered to the field of view and the background was minimized by adjusting the aperture. Cardiomyocytes were field stimulated at 0.5 Hz. The $Ca^{2+}$ recording was measured using the IonOptix IonWizard software, and the Calcium-Numeric-subtracted ratio of Fura-2 AM fluorescence (excitation at 340/380 nm and emission at 510 nm) was collected. Transients were collected for ∼60 seconds for each cell and the average values exported.

***FAM13B-GFP* EXPRESSION.** The FAM13B-eGFP fusion protein expression vector was constructed by VectorBuilder Inc (Cat#VB190426-1100mup). The elongation factor 1α short promoter drives the expression of the human FAM13B coding sequence (NM_016603.3) fused at its C-terminus to the enhanced green fluorescent protein (eGFP) coding sequence, with a Neomycin resistance gene inserted downstream of FAM13B-eGFP sequence connected by T2A Linker. iCell cardiomyocytes (Cellular Dynamics) were plated at a density of $5 \times 10^4$ cells per well into 0.1% gelatin-treated glass-bottom 96-well plate according to the manufacturer's instruction. The cells were maintained in iCell cardiomyocytes maintenance medium. Forty-eight hours later, the cells were transfected with the FAM13B-eGFP expression plasmid using ViaFect transfection reagent (Promega, Cat#E4981) at a 4:1 reagent-to-DNA ratio (vol:wt) and 0.1 μg plasmid DNA per well. Four to 6 days later, the cardiomyocytes were fixed with 10% phosphate-buffered formalin for 10 minutes at room temperature. After incubation with 0.1% Triton X 100 for 20 minutes to permeabilize the cell membrane, the cells were washed and incubated with Casein Blocker (ThermoFisher, Cat#37532) for 1 hour at room temperature. The cells were incubated with mouse anti-α-actinin primary antibody (1:500 dilution, Sigma-Aldrich, Cat#A7811) at 4°C overnight, and then with Alexa Fluor 568–labeled goat anti-mouse immunoglobulin G secondary antibody (1:500 dilution, ThermoFisher, Cat#A11004) for 2 hours at room temperature. Nuclei were counterstained with

Hoechst 33342 for 5 minutes and epifluorescent micrographs were obtained.

**RECOMBINANT HUMAN FAM13B PRODUCTION AND ACTIVITY.** A bacterial expression vector encoding human FAM13B with N-terminal 6 histidine (6xHis) and maltose binding protein (MBP) affinity tags was designed for soluble protein production (VectorBuilder, Cat#VB200129-1126cmr). Expression plasmids were transformed into *Escherichia coli* BL21 (DE3) Rosetta and protein expression was induced in shaking cultures by overnight incubation with 0.5 mM Isopropyl β-D-1-thiogalactopyranoside at 18°C. The resulting cellular pellet was resuspended in Buffer A (10 mM Tris [pH = 7.4] 350 mM NaCl with 1% protease inhibitor cocktail [Sigma, Cat#P8849]) and lysed by sonication. The resulting lysate was loaded on amylose resin (New England BioLabs, Cat#E8022), washed, and then eluted with Buffer A containing 10 mM maltose. The eluted 6xHis/MBP/FAM13B fusion protein was incubated with His-tagged Tobacco Etch Virus protease (New England Biolabs, Cat#P8112) overnight at 4°C to cleave the N-terminal affinity tags from FAM13B. The cleavage mixture was loaded on Ni Sepharose HP resin (GE Healthcare, Cat#GE17-5318-01) to remove the 6xHis tagged MBP, 6xHis tagged Tobacco Etch Virus protease, and any uncut fusion protein. The cleaved FAM13B protein was not bound to the Ni Sepharose and recovered in wash fractions containing phosphate-buffered saline + 20 mM NaCl and 30 to 40 mM imidazole. Fractions containing recombinant FAM13B were dialyzed against Buffer A and analyzed for purity by sodium dodecyl sulfate-polyacrylamide gel electrophoresis and Coomassie Blue staining. Authentication of the purified protein was determined by mass spectrometry. The samples were reduced by dithiothreitol, alkylated by iodoacetamide, and precipitated in cold acetone. Dried protein pellets were dissolved in 40 μL of 50 mM tri-ethyl ammonium bicarbonate with 1 μg sequencing grade trypsin and incubated at room temperature overnight. The liquid chromatography-mass spectrometry system was a ThermoScientific Fusion Lumos mass spectrometer system. The high-performance liquid chromatography column was a Dionex 15 cm × 75 μm Acclaim Pepmap C18, 2 μm, 100 Å reversed-phase capillary chromatography column. Five-microliter volumes of the extract were injected and the peptides were eluted by an acetonitrile/0.1% formic acid gradient. The digest was analyzed using the data-dependent multitask capability of the instrument acquiring full-scan mass spectra to determine peptide molecular weights and product ion spectra to determine amino acid sequence. The data were analyzed by using all CID spectra collected in the experiment to search the human SwissProtKB database with the search program Sequest. To determine if recombinant human FAM13B (rhFAM13B) had RhoGAP activity, a commercially available RhoGAP Assay kit (Cytoskeleton, Cat#BK105) was used. In brief, 4.6 μg FAM13B, or 3.9 μg of the positive control p50 RhoGAP, or a negative control without a RhoGAP were separately mixed with 6.1 μg of 4 well-characterized small Rho family GTPases (Ras, RhoA, Rac1, and Cdc42) and incubated with GTP for 20 minutes at 37°C. The reaction was terminated and GTPase activity was assessed by the generation of orthophosphate via the addition of the CytoPhos reagent. Absorbance at 650 nm was measured using a SpectraMax M2 microplate reader (Molecular Devices) to assess GTPase activity compared with the positive and negative control samples.

***FAM13B* KNOCKOUT MICE STUDIES.** All studies were performed according to protocols approved by the Cleveland Clinic or Ohio State University Animal Care and Use Committees. Frozen embryos of *Fam13b*$^{-/-}$ mice on the C57BL/6 background were obtained from the European Mutant Mouse Archive (strain EM:06267). The embryos were implanted into pseudo pregnant female mice by the Case Western Reserve University transgenic mouse core. Genotyping of the WT and knockout (KO) alleles was performed as specified by the Welcome Trust Sanger Institute using the common primer TGGCTATTTAATGTACCTAGAAAATGG, the WT allele-specific primer AAACAAAAGCTTGCATGTAGCA, and the KO allele-specific primer TCGTGGTATCGTTATGCGCC. The *Fam13b*$^{-/-}$ mice were mated to C57BL/6J mice to create *Fam13b*$^{-/+}$ $F_1$ mice, which were brother mated to generate *Fam13b*$^{-/-}$ and *Fam13b*$^{+/+}$ mice that were the founders of the mice used in this study. Mice were fed a standard laboratory diet (Envigo, Cat#2018). All mice used in the current study, including those used for surface electrocardiographs (ECG), echo, heart weight, and histology, were at least 1 year old before study. The choice to use 1-year-old mice was based on a published mouse pacing study in which old (>52 weeks) vs young (12- to 16-week-old) mice had increased pacing-induced atrial arrhythmogenicity.[23] Echocardiography was performed on isoflurane anesthetized mice using a VEVO 2100 (FujiFilm VisualSonics) echocardiographic machine as previously described.[24] M-mode recording was used to obtain cardiac functional parameters. ECG and intracardiac recordings were obtained, by an investigator blinded to the mouse genotypes, in mice anesthetized with 2%

to 3% isoflurane with body temperature maintained between 36.5 °C and 37.5 °C by a thermally controlled heating pad. After a 5-minute stabilization period, the basal ECGs were obtained for another 5 to 10 minutes. Surface ECGs were continuously obtained during the pacing study described in the following. Surface ECG analysis was performed as previously described, using custom-built software kindly shared by Dr David Filgueiras-Rama (CNIC Madrid, Spain), and QTc values were calculated at $QT/(RR/100)^{1/2}$.[25] For pacing-induced arrhythmia studies, an electrophysiology catheter (Transonic, 1.1F size) with 8 electrodes was inserted through the jugular vein and advanced into the right atrium and ventricle in order to obtain intracardiac recordings.[26] Power analysis for heart function and surface ECG was done before performing these studies using GraphPad Instat software; we calculated 80% power to detect a 24% change using a parametric *t*-test with n = 12 per group and an estimated coefficient of variation of 20%. Programmed electrical stimulation was performed as previously described with some modifications.[27] Atrial stimulation was achieved by rectangular impulses of 2 ms delivered at twice the pacing threshold milliamperes. A modified 2-phase burst-stimulation protocol was used to induce atrial arrhythmia: 10 phase 1 preconditioning stimuli (cycle length 60 ms) was followed by 20 phase 2 burst stimuli (cycle length 5 ms) with delay of 1 minute between preconditioning and burst-stimulation applications. This sequence of programmed electrical stimulation was repeated 10 to 16 times before and after intraperitoneal injection of 1.5 mg/kg isoproterenol during a 1-minute interval. Atrial arrhythmia, for simplicity labeled as AF, was defined as the occurrence of rapid and fragmented atrial electrograms (lack of regular P waves) with irregular ventricular rhythm (irregular RR intervals), all lasting at least 3 seconds. Ventricular arrhythmia was defined as transient variability in the contractile waveform in comparison with its baseline pattern. Premature ventricular contraction was defined as early contraction before relaxation. LabScribe ECG Analysis software (iWorx RA834) was used for the intracardiac recordings and assessment. Before performing the pacing studies, we performed a power calculation using GraphPad Instat software for a chi-square test assuming pacing-induced atrial arrhythmia in control mice at 10% frequency. We determined 80% power to observe an increase in atrial arrhythmia incidence to 60% frequency with N = 12.

**STATISTICS.** Aside from eQTL analysis (described previously), all statistics were performed using GraphPad Prism 9 software. All data were analyzed for normality by the Shapiro-Wilk and D'Agostino & Pearson tests; if passing either test, mean ± SD are shown, if not normally distributed medians with 25th and 75th percentiles (Q1-Q3) are shown with box plots or by indicating the medians within dot plots, and nonparametric tests were employed. Comparisons between 2 groups were performed by Student's *t*-test or Mann-Whitney test for normally and non-normally distributed data, respectively. Comparisons for more than 2 groups were performed by analysis of variance (ANOVA) with Tukey post hoc tests for multiple pairwise comparisons. Statistical significance was defined as a $P$ value ≤0.05 in 2-sided tests. Categorical data were analyzed by Fisher's exact test. FDR q-values were calculated using the Benjamini-Hochberg method. To exclude obvious outlier data, the Grubbs test was applied with $\alpha = 0.05$ using the online GraphPad calculator. Any excluded values are denoted in the figure legend.

## RESULTS

**AFRICAN ANCESTRY eQTL ANALYSIS FOR FAM13B GENE EXPRESSION.** Our published LAA RNAseq-eQTL analysis focused on 235 and 30 subjects with European ancestry and African ancestry, respectively.[5] In the European ancestry subjects, we showed that the lead chr 5q31 GWAS SNP at that time, rs2040862, was a strong eQTL for expression of the *FAM13B* gene ($P = 7 \times 10^{-30}$). However, in European ancestry populations, this SNP is in strong LD with many other SNPs that have similar eQTL $P$ values.[5] Although our African American cohort was small, we were able to detect a significant eQTL for *FAM13B* expression. The rs17171731 SNP, located ~19 kb upstream of the major *FAM13B* transcription start site, stood out with an eQTL $P$ value ~10-fold stronger than the other SNPs in this region (**Figures 1A and 1B**) ($P = 2.63 \times 10^{-5}$). rs17171731 is in high LD with the GWAS SNP rs2040862 in our European ancestry subjects ($r^2 = 0.96$), but the LD between these 2 SNPs is much weaker in African ancestry subjects ($r^2 = 0.45$, HaploReg 4.1 using 1000 Genomes phase 1 data). The rs17171731 major allele is C, and the minor allele, G, frequency is 19% in European and 9% in African individuals (dbSNP build 155).

**ANALYSIS OF HUMAN FAM13B EXPRESSION BY RNAseq.** The GTEx portal (queried on August 23, 2022) shows that *FAM13B* expression is widespread in human tissues with the highest expression in the large arteries (tibial, coronary, and aorta at 37 to 39 transcripts per million). *FAM13B* is expressed in the right atrial appendage at 9.5 transcripts per million

**FIGURE 1 Identification of the AF Causal Gene and Candidate SNP**

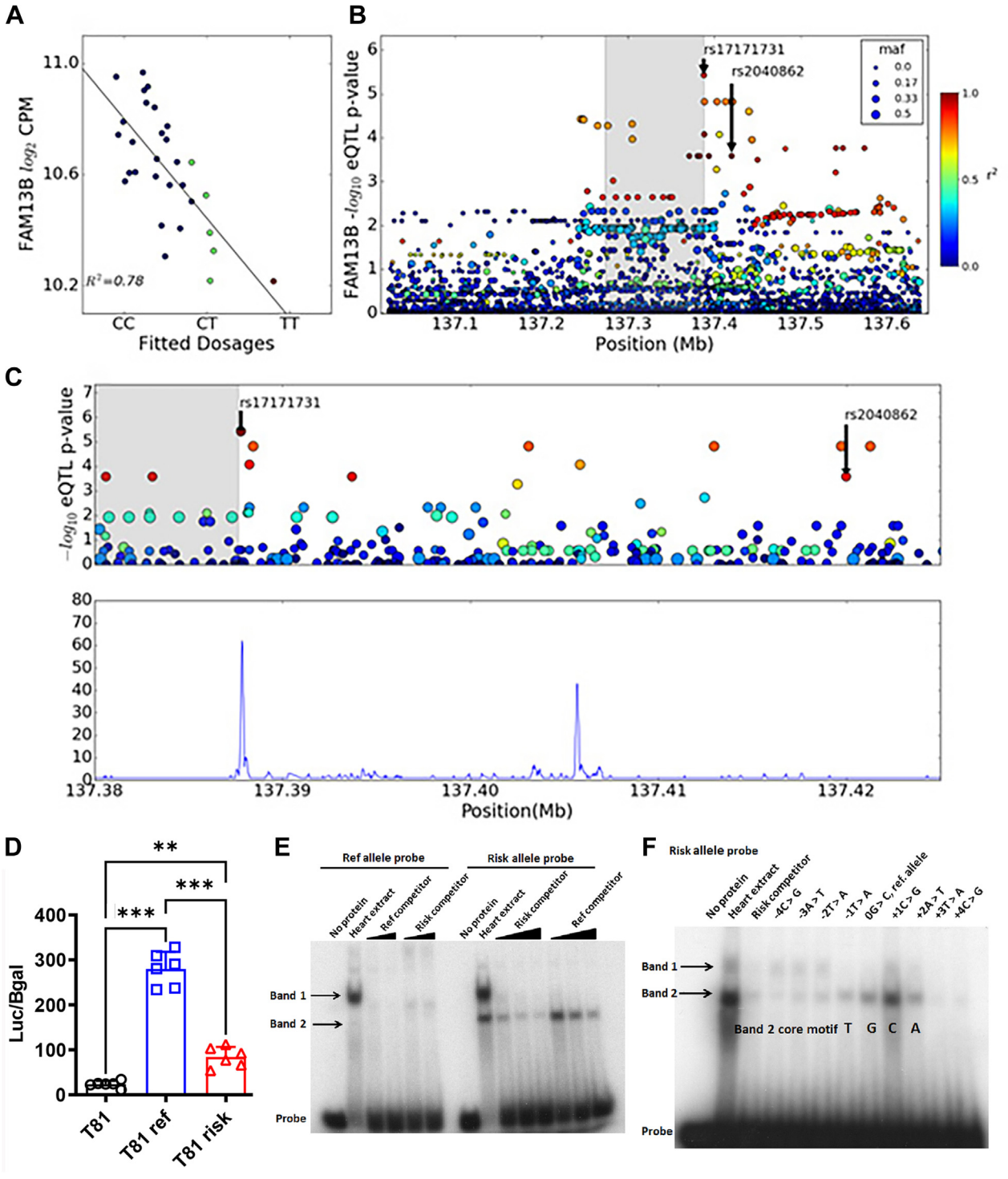


*Continued on the next page*

(LAA tissue is not included in the GTEx project). To get insight into which cells in the LA express *FAM13B*, we analyzed the single-nuclei RNAseq data from the 6 LA samples described in Tucker et al.[14] Our UMAP plot shows that *FAM13B* is expressed in all cell types (Supplemental Figure 1A). Because of low sequence depth in each nucleus, one does not expect to detect expression in every cell within each cluster. We calculated the median % of *FAM13B* expressing cells in atrial cardiomyocytes were approximately equal to vascular smooth muscle > adipocytes > fibroblasts II > macrophages> neuronal > all other cell types (Supplemental Figure 1B). We also ranked the cell clusters by *FAM13B* gene expression counts per million, and found expression highest in vascular smooth muscle > atrial cardiomyocytes >macrophages > adipocytes > fibroblasts II > pericytes > all other cell clusters (Supplemental Figure 1C).

**FUNCTIONAL STUDIES OF THE FAM13B CANDIDATE CAUSAL SNP.** Based on the *cis*-eQTL analysis (**Figures 1A and 1B**) and DNaseI hypersensitivity in human fetal heart (**Figure 1C**), we identified rs17171731 as the top candidate causal SNP regulating *FAM13B* gene expression. To detect enhancer activity in this region, we subcloned 26-mer oligos containing the reference or risk alleles of rs17171731 (Supplemental Table 1) into a luciferase reporter plasmid driven by a minimal viral thymidine kinase promoter. After transfection into iCMs, we observed that the risk allele had weak enhancer activity, whereas the reference allele had 3.3-fold stronger activity vs the risk allele ($P < 0.001$) (**Figure 1D**).

We then performed electromobility shift assays using $^{32}$P-labeled 26-mer oligos surrounding the rs17171731 SNP (**Figure 1E**). Incubation of the reference allele probe with human heart nuclear extract yielded 1 strongly shifted fragment (Band 1), and the risk allele yielded both Band 1 and a smaller shifted fragment (Band 2). Band 1 was effectively competed off of both probes with excess unlabeled reference or risk oligos; however, Band 2 was competed off more effectively with the risk vs reference oligo. Using a different lot of heart nuclear extract that had more prominent Band 2 vs Band 1 shifts, along with the risk allele probe, we performed competition studies using 9 unlabeled oligos (Supplemental Table 1) with single bp changes extending ±4 bp from the rs17171731 SNP site (**Figure 1F**). We determined that the central sequence motif required for the Band 2 shift was TGCA, with the rs17171731 risk allele representing the G of this motif. We searched the JASPAR transcription factor motif database[28] for TGCA binding factors with scores >93.5 and narrowed our list to those that were expressed in LAA based on our RNAseq data,[5] which yielded the following 7 factors: ATF4, POU2F1, SOX4, SOX8, ABI3, MTF1, and POU2F2. Commercially available antibodies against these proteins did not supershift or block Band 2 formation (Supplemental Figure 2); thus, we did not identify the heart nuclear protein(s) responsible for the Band 2 shift that shows higher affinity for the rs17171731 risk allele. Given that both alleles showed net enhancer activity in the reporter gene transfection study, we interpret our gel shift results to indicate that Band 1 represents an enhancer complex, and Band 2 represents a silencer complex.

To further investigate the regulatory impact of the motif containing rs17171731, we used CRISPR-Cas9-mediated nonhomologous end joining to target the rs17171731 for indel mutation. An sgRNA targeting rs17171731 was transfected via electroporation into pluripotent stem cells expressing Cas9. Twelve clonally derived cell lines were sequenced yielding 5 with no mutations, 6 heterozygous with 1 indel and 1 WT allele, and 1 clone harboring 2 different single-bp

**FIGURE 1 Continued**

(A) Partial regression plot showing the effect of the genome-wide association study (GWAS) single-nucleotide polymorphism (SNP) rs2040862 on left atrial appendage (LAA) expression of the *FAM13B* gene in African American subjects. Blue dots are subjects homozygous for the major allele, green dots are heterozygotes, and red dots are homozygous for the minor allele ($r^2 = 0.78$ Pearson's correlation, q value = 0.01). (B) Expression quantitative trait loci (eQTL) *P* values and linkage disequilibrium (LD) relationship (color scale) with the GWAS SNP rs2040862 in the region around *FAM13B* in African American subjects, identifying rs17171731 as the top eQTL SNP ($P = 2.63 \times 10^{-5}$). The gray-shaded area represents the longest *FAM13B* gene (transcribed from left to right) in Ensembl, but the LAA transcript starts ~19 kb proximal to rs17171731. (C) Zoom in on *FAM13B cis*-eQTL for African American subjects with LD relationships for rs17171731 (top). The SNP rs17171731 occurs in a DNaseI hypersensitivity peak, whereas the atrial fibrillation (AF) GWAS SNP rs2040862 does not (bottom, Roadmap Epigenomics Project data for human fetal heart). (D) Reporter gene transfection into stem cell–derived cardiomyocytes (iCMs) showing the effects of oligonucleotides for the reference and risk allele of rs17171731 on luciferase/β-galactosidase expression (mean ± SD; ***$P < 0.001$ and **$P < 0.01$ by 1-way analysis of variance [ANOVA] with Tukey posttest, N = 6 biological replicates). (E) Cardiomyocyte nuclear extract gel shift assay with probes for the reference and risk allele of rs17171731, demonstrating that both probes shift band 1, but only the risk allele shifts band 2. Increasing concentrations of the reference and risk allele unlabeled competitors were added as indicated (10-, 25-, and 50-fold molar excess). (F) Gel shift assay of the AF risk allele using unlabeled competitors (100-fold molar excess) containing 1-base pair changes centered on the rs17171731 SNP, yielding the core sequence element of TGCA for the band 2 gel shift.

**FIGURE 2 CRISPR Editing of rs17171731**

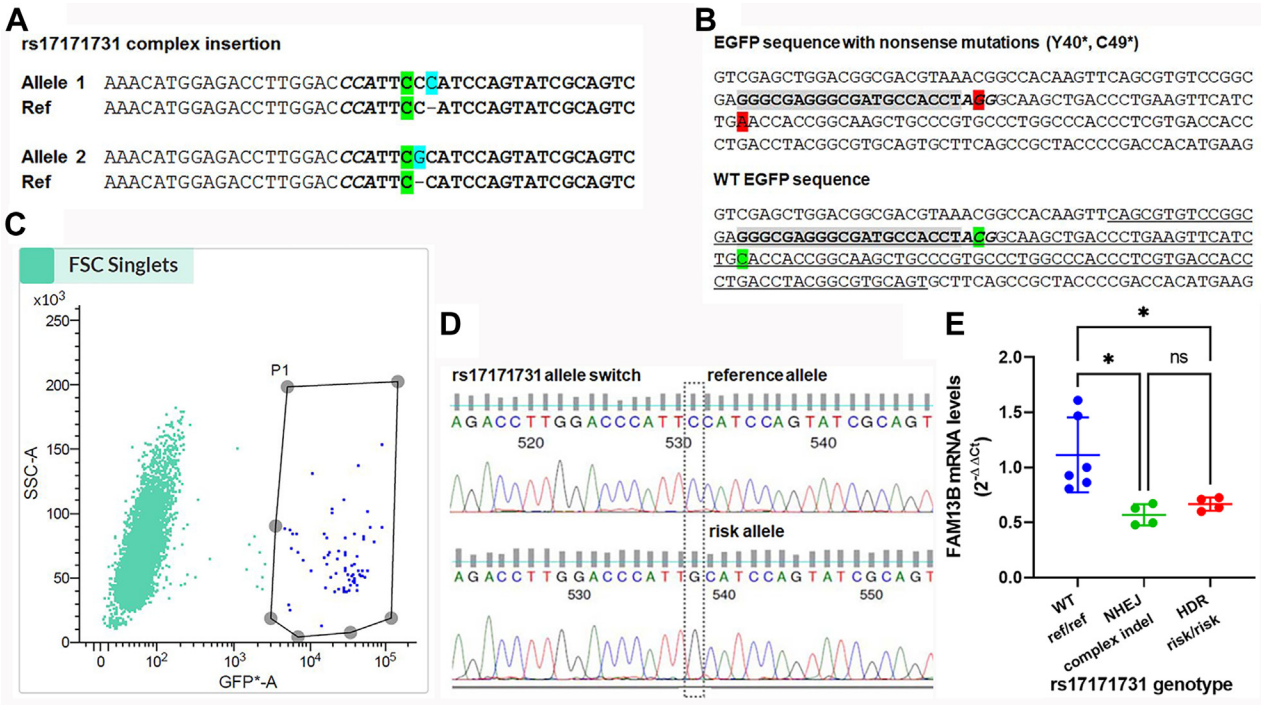


(A) Sanger sequencing of complex insertion into rs17171731 site via nonhomologous end joining (NHEJ). Bold italic font, PAM sequence opposite strand; bold font, single guide RNA (sgRNA) target sequence; green highlight, rs17171731 reference allele; blue highlight, inserted base pairs. (B) Strategy to select for homology-directed repair (HDR) co-editing. An enhanced green fluorescent protein (eGFP) expression plasmid was mutated to include 2 stop codons and stably transfected into stem cells (top). Sequence of repaired eGFP after sgRNA and donor oligo transfection to correct stop codons and alter the PAM sequence to prevent re-editing (bottom). Gray highlight, sgRNA target sequence; bold italic font, PAM sequence; red highlight, Y40* and C49* stop codon mutations; underlined sequence, single-strand HDR repair oligo donor; green highlight, corrected eGFP sequence and altered PAM site. (C) Fluorescent activated cell sorting after eGFP and rs17171731 HDR co-editing, yielding 0.69% eGFP+ cells used for clonal growth. (D) Sanger sequencing of the rs17171731 region in the WT stem cells (top, homozygous reference allele) and co-edited cells (bottom, homozygous risk allele). (E) *FAM13B* messenger RNA expression in iCMs from unedited cells (wild type [WT], reference alleles), NHEJ edited cells (complex insertion), and HDR edited cells (risk alleles). Each point represents the mean of technical triplicates from 4 to 6 biological replicates (independent wells) of iCMs per genotype (dot plot with mean ± SD; *$P < 0.05$ by 1-way ANOVA with Tukey post hoc test; ns, not significant). Abbreviations as in Figure 1.

insertions in this region (complex insertion) (Figure 2A). To obtain stem cells with precise editing, changing the homozygous reference to homozygous risk allele, we used an HDR cotransfection strategy to select HDR-competent cells via a GFP double nonsense to GFP sense reporter system, yielding 0.69% $GFP^+$ cells by flow cytometry (Figures 2B and 2C). Forty-eight clonally derived cell lines were screened by Sanger sequencing, of which most were heterozygous for the reference and risk alleles, and 1 was homozygous for the risk allele (Figure 2D). WT, complex insertion, and homozygous risk allele stem cells were differentiated into iCMs. Compared with WT cells homozygous for the rs17171731 reference allele, *FAM13B* mRNA expression decreased by ~50% in iCMs derived from either the complex insertion or homozygous risk allele cell lines (Figure 2E) ($P < 0.05$ vs WT cells by ANOVA with Tukey's multiple comparison test). Thus, the rs17171731 risk vs reference allele yielded decreased expression of the endogenous *FAM13B* gene in otherwise isogenic iCMs, in agreement with the results of the reporter gene transfection studies (Figure 1D), and the human LAA eQTL study (Figure 1B).

**KD OF FAM13B.** *FAM13*B (prior gene name C5ORF5[6]) is a member of the RhoGAP gene family. In silico analysis of the FAM13B RhoGAP domain indicates that 2 highly conserved putative GTPase catalytic residues are altered in the FAM13B protein, potentially yielding a noncatalytic protein.[6] To begin to evaluate the mechanism whereby FAM13B impacts atrial arrhythmogenesis, RNAseq and electrophysiology studies

were performed to assess the effect of *FAM13B* KD via siRNA transfection vs Scr siRNA on iCell cardiomyocytes, which are highly enriched in cardiomyocyte composition with a mature and organized sarcomere structure. We evaluated 3 siRNAs, and used the one with the most efficient KD. Four days after *FAM13B* siRNA transfection, we observed 77% KD of *FAM13B* mRNA expression by qPCR (**Figure 3A**). RNA-seq analysis of the *FAM13B* and Scr siRNA-treated cells revealed that expression levels of 1,156 genes were significantly altered after *FAM13B* KD (FDR adjusted $P < 0.10$, n = 3 per condition) (Supplemental Table 3), with the top 20 most significant changes in gene expression shown in **Table 1**. Although expression levels of most prominent atrial ion channel pore subunits were not significantly affected by *FAM13B* KD, expression of *SCN2B,* which encodes a beta-subunit of the cardiac sodium channel, was the 11th strongest regulated transcript, and it was downregulated 2.2-fold by *FAM13B* KD (**Table 1**). Ingenuity Pathway analysis revealed that the top canonical pathway was calcium signaling ($P$ = 1.19E-03), which contains 5 genes strongly upregulated by *FAM13B* KD (Supplemental Figures 3A and 3B). The top 5 empirical networks from Ingenuity Pathway analysis are shown in Supplemental Figure 3C, and *SCN2B* is a member of the strongest empirical network (**Figure 3B**). Gene set enrichment analysis identified 86 gene sets altered by *FAM13B* KD (FDR <0.1) (Supplemental Table 4). The 2 strongest sets were Kyoto Encyclopedia of Genes and Genomes: Dilated Cardiomyopathy (downregulated, 62 genes in set, FDR = 3.94E-03) and Reactome: Constitutive Signaling Overexpressed ERBB2 (upregulated, 10 genes in set, FDR = 0.017). ERBB2 was previously identified as an AF-associated biomarker.[29] Of interest because *FAM13B* is in the RhoGAP gene family, there were also 3 Rho GTPase activation gene sets among the top 86 sets. Two gene sets containing *SCN2B* (Reactome: Phase 0 Rapid Depolarization and Reactome: Sensory Perception) were among the top sets. A common off-target effect of some siRNAs is the induction interferon responsive genes; here the Scr siRNA may have had this property, as 2 interferon-related gene sets were both downregulated by *FAM13B* KD (Supplemental Table 4).

As *SCN2B* expression was highly repressed after *FAM13B* KD, patch clamp studies of *FAM13B* KD iCell cardiomyocytes focused on measurement of sodium current ($I_{Na}$) density (**Figures 3C and 3D**), steady-state inactivation (**Figures 3E and 3F**), and late sodium current ($I_{NaL}$) (**Figures 3G and 3H**). *FAM13B* KD did not significantly impact the peak sodium current density (**Figure 3D**). *FAM13B* KD increased the $V_{1/2}$ for the steady-state inactivation of the $I_{Na}$ by 2.7 mV (**Figure 3F**), and although this effect did not reach $P < 0.05$ by *t*-test ($P = 0.139$), a 2-way ANOVA test showed a significant difference between the curves ($P = 0.002$ for interaction between siRNA treatment and voltage). Cell capacitance was not significantly different between groups (KD: 39.5 ± 6.5 pF vs Scr 36.4 ± 4.5 pF). Late sodium window current density ($I_{NaL}$) was evaluated using a ramp clamp protocol (**Figure 3G**). There was a tendency for $I_{NaL}$ density to be larger in the *FAM13B* KD cells compared with the Scr siRNA control (−1.73 ± 0.33 vs −1.24 ± 0.13 pA/pF, $P = 0.20$). When subdivided by cell capacitance above and below the median value (37.7 pF), the difference in $I_{NaL}$ density between KD and Scr control groups was significant for the lower capacitance cells ($P = 0.044$), but not for the higher capacitance cells ($P = 0.88$). The ratio of $I_{NaL}$/peak $I_{Na}$ was significantly increased in the *FAM13B* KD cells, regardless of cell capacitance (**Figure 3H**) ($P = 0.025$).

As calcium signaling was the top canonical pathway associated with *FAM13B* KD, $Ca^{2+}$ transients were also analyzed in Scr and *FAM13B* KD iCell cardiomyocytes paced at 0.5 Hz (**Figures 3I and 3J**). *FAM13B* KD led to significantly lower peak cytosolic $Ca^{2+}$ amplitude ($P < 0.001$), significantly shorter 50% time to peak cytosolic $Ca^{2+}$ ($P = 0.047$), and significantly delayed 50% time to baseline ($P < 0.001$). The faster release of $Ca^{2+}$ from the sarcoplasmic reticulum after *FAM13B* KD is consistent with *FAM13B* KD leading to a 2.8-fold increase in calsequestrin 2 (*CASQ2*) mRNA (adj $P$ = 8.64E-3) (**Table 1**), encoding the major $Ca^{2+}$ storage protein, which may lead to increased sarcoplasmic reticulum $Ca2^{+}$ stores. The delayed reuptake of $Ca^{2+}$ after *FAM13B* KD is also consistent with a modest but significant 19% decrease in *ATP2A2* mRNA, encoding the major cardiac Sarcoplasmic/Endoplasmic Reticulum Calcium ATPase 2 (SERCA2) $Ca^{2+}$ pump isoform, after *FAM13B* KD (adj $P$ = 0.049) (Supplemental Table 3).

**FAM13B LOCALIZATION AND ENZYME ACTIVITY.** To gain more insight into the FAM13B mechanism of action, we transfected different cell types with a FAM13B-GFP fusion protein construct. On transfection into noncardiomyocyte HEK293 and human pluripotent stem cells, we observed a few GFP+ cells 2 days after transfection, but these cells were compact, round, and poorly attached, and died by day 4, such that no GFP+ cells remained on the dish. However, after transfection into iCell cardiomyocytes, we observed robust GFP+ staining in the sarcomeres and light expression on the plasma

**FIGURE 3 Functional Consequences of *FAM13B* Knockdown**

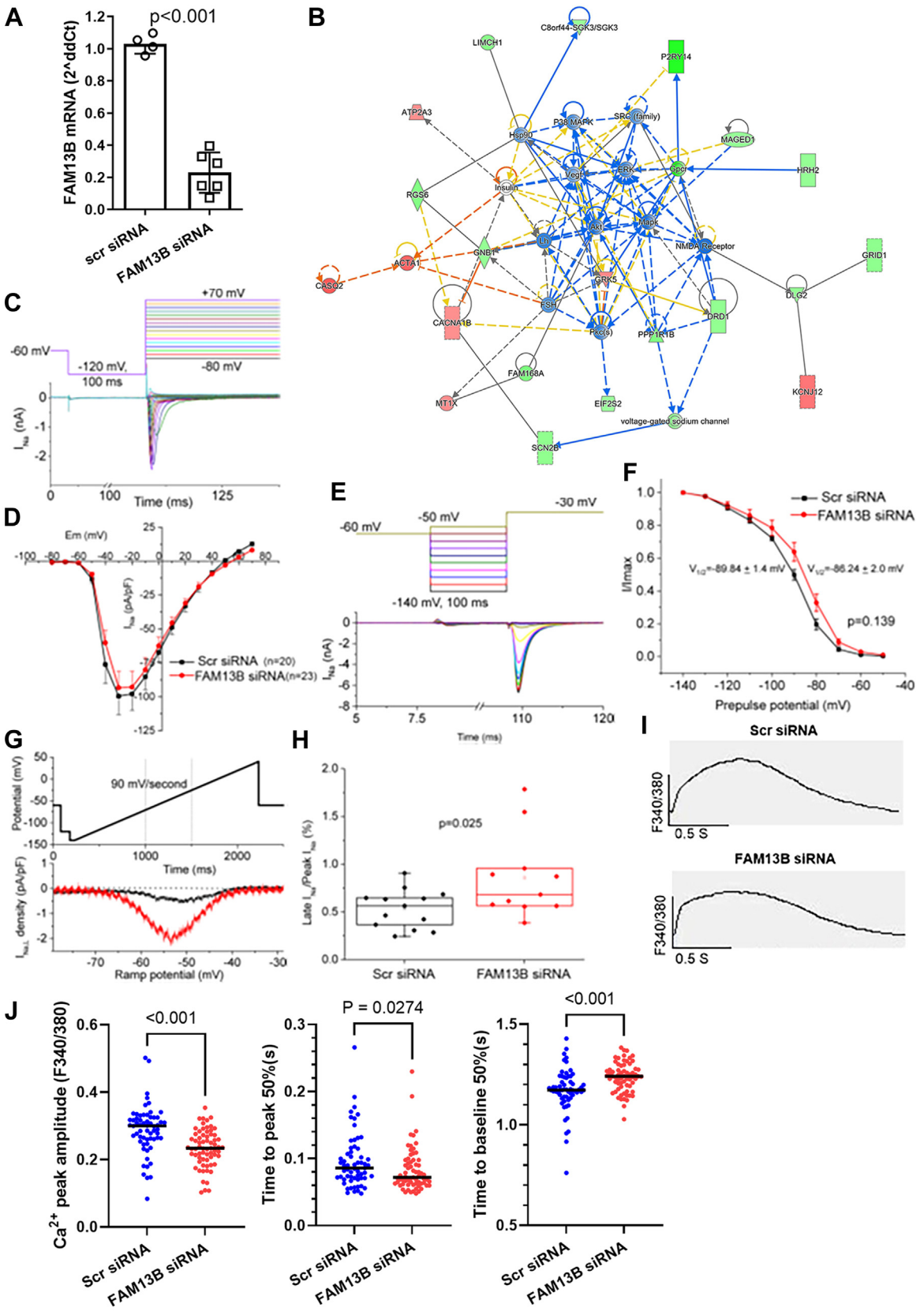


*Continued on the next page*

membrane (Figure 4A). We observed strong FAM13B-GFP signal colocalized with or adjacent to α-actinin, a marker for the Z-disc, detected by immunofluorescence (Figures 4B to 4D). FAM13B-GFP was not strongly colocalized with the Sarcoplasmic/Endoplasmic Reticulum Calcium ATPase 2 (SERCA2), a marker for the sarcoplasmic reticulum (Supplemental Figure 4). As a control, eGFP alone was transfected into iCell cardiomyocytes, which yielded nuclear and stress fiber, but not sarcomere, localization (Supplemental Figure 5).

We made rhFAM13B protein in *E. coli*, but it was not soluble as an N-terminal 6xhis-tagged protein. The N-terminal 6xhis-MBP-FAM13B fusion protein was recovered in the soluble fraction. The fusion protein was purified yielding a protein that was >82% pure by densitometry after sodium dodecyl sulfate-polyacrylamide gel electrophoresis (Figure 4E, first lane after Ni column). Mass spectrometry identified the major protein as FAM13B with 96 peptides identified representing 84% sequence coverage. The major contaminating protein was MBP. The rhFAM13B was tested for RhoGAP activity using 4 different rho proteins, but no activity was detected, whereas a positive control p50 RhoGAP protein increased GTPase activity for 3 of the 4 Rho proteins (Figure 4F).

***FAM13B* KO MICE HAVE PROLONGED P-WAVE AND QT INTERVAL DURATION AND INCREASED PACING-INDUCED ARRHYTHMIA.** Because the chr 5q31 AF risk allele is associated with decreased *FAM13B* mRNA expression in human LAA, we decided to evaluate the *Fam13b* KO mouse model. *Fam13b*$^{-/-}$ mice were viable and fertile. Surface ECG did not detect any spontaneous arrhythmia in young *Fam13b*$^{-/-}$ mice, so we decided to study them and their WT controls at 1 year of age. Ejection fraction and left ventricular mass, as assessed by echocardiography, was not altered in the KO vs WT mice (Figure 5A). Postmortem analysis of heart weights (with or without controlling for tibia length) showed no significant genotype effect in either males or females (Figure 5B). Furthermore, postmortem heart appearance and histology were similar in the KO vs control mice (Figures 5C and 5D). Masson's trichrome staining did not detect abundant fibrosis in the ventricular or atrial myocardium in either WT or KO hearts (Figure 5D, higher magnification in Supplemental Figure 6). In the male mice, surface ECG showed no significant effect on RR interval; however, durations of the QRS, QT, QT corrected for RR interval, and P-wave were all significantly longer in the KO vs WT mice (Figure 5E). For example, the median durations for corrected QT and the P-wave were 29% ($P < 0.001$) and 34% ($P = 0.004$) longer in the KO mice, respectively (nonparametric Mann-Whitney tests). In the female mice, the same direction was observed although nonsignificant, with longer durations of the QT, corrected QT, and P-wave in the KO vs WT mice (Figure 5E).

Intracardiac pacing and recording under basal and isoproterenol (IsoP) stress conditions were performed to determine arrhythmia induction susceptibility (Figures 6A to 6D). AF was diagnosed if the RR interval was variable and the P-wave lost its clear shape and rhythmicity (Figures 6A and 6B), which we quantified both per mouse (yes or no if a mouse had any AF incidents) and per pacing trial (counting the number of trials with AF incidence vs sinus rhythm for all mice in a group). Some examples of resting ECGs for WT and KO mice are shown in Supplemental

**FIGURE 3 Continued**

(A) Quantitative reverse transcriptase-polymerase chain reaction verification of small interfering RNA (siRNA) *FAM13B* knockdown in iCell cardiomyocytes normalized to *ACTC1* messenger RNA (mRNA) relative to the scrambled (Scr) siRNA (mean ± SD, $P < 0.001$ by 2-tailed *t*-test, n = 4-6 biological replicates [each from technical triplicates] from 2 independent experiments, 1 Scr outlier was removed using the Grubbs test). (B) The strongest empirical network for *FAM13B* KD identified by Ingenuity Pathway analysis, which included the *SCN2B* gene encoding a subunit of the voltage-gated sodium channel. Green indicates repression and red indicates induction upon *FAM13B* knockdown, with the color saturation indicating the fold effect. (C) Representative sodium current ($I_{Na}$) traces and voltage-clamp protocol. A 100-ms pre-pulse to −120 mV was used from a holding potential of −60 mV. Depolarizing voltage steps from −80 to +70 mV were applied in 10-mV increments. (D) Summary $I_{Na}$-V plot for scramble (n = 20) vs *FAM13B* knockdown (n = 23) recordings. (E) Inactivation protocol and representative $I_{Na}$ traces. As in (C), resting potential was −60 mV, with a 100-ms pre-pulse used to partially recover channels from inactivation, using pre-pulse potentials from −140 to −50 mV in 10-mV steps. $I_{Na}$ was recorded with a step to −30 mV. (F) $I_{Na}$ currents were normalized to those recorded at −140 mV (I/Imax). A Boltzmann function was used to fit the half-inactivation potential ($V_{1/2}$). A subset of the cells in (D) were characterized (scramble n = 9, knockdown n = 7, the $V_{1/2}$ values were compared by Student's *t*-test). (G) Slowly inactivating $I_{Na}$ ($I_{na}$) was recorded using a 2s ramp clamp protocol from −140 to +50 mV (90 mV/second). Representative current traces normalized to cell capacitance are shown over the potential range −80 to −30 mV for a scramble (black) and *FAM13B* knockdown (red) cardiomyocyte. The baseline subtracted peak negative amplitude of the window current recorded in this range was used as a measure of $I_{NaL}$. (H) A subset of the cells in (D) were evaluated using the (G) protocol (dot plot and box plot of median and IQR; $P = 0.025$, Mann-Whitney test). The percent of $I_{NaL}$ to peak $I_{Na}$ is plotted from scramble (n = 11) vs *FAM13B* knockdown (n = 13) cells. (I) Time-averaged $Ca^{2+}$ traces from representative iCell cardiomyocytes transfected with Scr siRNA (upper) or *FAM13B* siRNA (lower) paced at 0.5 Hz. (J) Compared with Scr siRNA transfected cells (blue symbols, n = 61 biological replicates), *FAM13B* siRNA transfected cells (red symbols, n = 67 biological replicates) showed a significantly lower peak Ca2+ amplitude (right side), shorter time to peak 50% (center) and longer time to baseline 50% (left side). Data pooled from 2 independent experiments, black lines show median values, *P* values were determined by the Mann-Whitney test.

**TABLE 1 Twenty Most Significantly Regulated Genes After *FAM13B* Knockdown**

| Gene Symbol | Entrez Gene ID | Ensembl Gene ID | Gene Length (bp) | Log2 Fold Change (FAM13B siRNA vs Scr siRNA) | AveExpr (Log2 counts/ million) | *P* Value | Q Value |
|---|---|---|---|---|---|---|---|
| EPPK1 | 83481 | ENSG00000261150 | 7,273 | 1.51 | 7.56 | 9.99E-07 | 3.09E-03 |
| TBC1D8 | 11138 | ENSG00000204634 | 4,147 | −0.97 | 6.49 | 1.12E-06 | 3.09E-03 |
| HDDC2 | 51020 | ENSG00000111906 | 1,615 | −1.14 | 4.83 | 1.12E-06 | 3.09E-03 |
| MYH11 | 4629 | ENSG00000133392 | 6,942 | 1.84 | 3.25 | 4.32E-07 | 3.09E-03 |
| SLC4A4 | 8671 | ENSG00000080493 | 8,010 | −1.03 | 5.33 | 1.74E-06 | 3.83E-03 |
| TCAP | 8557 | ENSG00000173991 | 963 | −1.06 | 8.37 | 5.38E-06 | 7.46E-03 |
| RASD1 | 51655 | ENSG00000108551 | 1,746 | −0.88 | 4.64 | 5.99E-06 | 7.46E-03 |
| FAM120B | 84498 | ENSG00000112584 | 3,239 | −0.90 | 4.33 | 6.74E-06 | 7.46E-03 |
| SLC41A1 | 254428 | ENSG00000133065 | 4,854 | −0.93 | 6.40 | 7.78E-06 | 7.46E-03 |
| ACE2 | 59272 | ENSG00000130234 | 3,507 | 1.30 | 6.56 | 8.12E-06 | 7.46E-03 |
| SCN2B | 6327 | ENSG00000149575 | 4,922 | −1.14 | 4.31 | 7.33E-06 | 7.46E-03 |
| SCML1 | 6322 | ENSG00000047634 | 2,911 | −1.55 | 3.09 | 4.85E-06 | 7.46E-03 |
| PDE4DIP | 9659 | ENSG00000178104 | 12,539 | −1.15 | 10.00 | 9.20E-06 | 7.80E-03 |
| XRCC4 | 7518 | ENSG00000152422 | 1,704 | 0.90 | 7.20 | 1.21E-05 | 8.41E-03 |
| FAM13B | 51306 | ENSG00000031003 | 5,624 | −2.17 | 5.40 | 1.17E-05 | 8.41E-03 |
| MT1X | 4501 | ENSG00000187193 | 404 | 1.04 | 3.28 | 1.22E-05 | 8.41E-03 |
| KRT80 | 144501 | ENSG00000167767 | 3,894 | 0.79 | 4.74 | 1.38E-05 | 8.64E-03 |
| CASQ2 | 845 | ENSG00000118729 | 2,702 | 1.51 | 9.30 | 1.55E-05 | 8.64E-03 |
| SLC40A1 | 30061 | ENSG00000138449 | 3,355 | −1.29 | 5.68 | 1.60E-05 | 8.64E-03 |
| DRAM2 | 128338 | ENSG00000156171 | 1,886 | 0.71 | 5.18 | 1.74E-05 | 8.64E-03 |

AveExpr = average gene expression; bp = base pairs; Scr = scrambled; siRNA = small interfering RNA.

Figure 7. Under basal conditions, there were no significant differences found for KO vs WT male (RR = 2.55, $P = 0.47$) and female (RR = 1.65, $P = 0.45$) mice to have increased susceptibility to pacing-induced AF (**Figure 7A**), although the relative risk direction was consistent with increased risk in the KO mice. AF susceptibility increased under IsoP stimulation, with no *Fam13b* genotype effect in the males (RR = 0.96), whereas the KO vs WT females were significantly more susceptible to AF (RR = 2.85, $P = 0.035$) (**Figure 7A**). Per pacing trial, AF was induced more frequently in KO vs controls for males and females under basal conditions, and for females under IsoP stimulation (**Figure 7B**). In addition to AF, we also observed some instances of ventricular arrhythmia, appearing most frequently as premature ventricular contractions (**Figures 6C and 6D**). Although this was not common, it only occurred in the KO mice, showing statistical significance for the males under isoproterenol stimulation ($P = 0.036$), and in both sexes and conditions combined ($P = 0.004$) (**Figure 7C**).

## DISCUSSION

Our prior LAA RNAseq analysis identified the chr 5q31 AF GWAS SNP rs2040862 at a locus previously attributed to *WNT8A,* which is in fact a strong eQTL for *FAM13B* expression, while *WNT8A* is not expressed in human LAA.[5] The minor allele of rs2040862 is the AF risk allele, and this allele is associated with decreased expression of *FAM13B*. The *FAM13B* gene encodes an uncharacterized protein containing a RhoGAP domain.[6] The eQTL plots for LAA *FAM13B* expression in African American subjects and a DNaseI hypersensitivity peak map in fetal heart tissue allowed us to identify rs17171731 as a top candidate functional SNP. Our reporter gene transfection and CRISPR allele switching studies show that rs17171731 is a causal variant, with the risk allele having decreased enhancer activity, in the same direction as observed in human LAA tissue. We do not mean to imply that rs17171731 is causal for the AF phenotype, as clearly it is only a weak genetic susceptibility factor; instead, we claim that rs17171731 is the SNP responsible for the AF GWAS locus at chr 5q31 because of its direct effect on *FAM13B* expression.[30] A different SNP at chr. 5q31 (rs1004989) that was previously associated with the electrocardiographic QT-interval was found to be a significant eQTL for *FAM13B* expression in left ventricle tissue samples;[30] however, rs1004989 is not in LD with rs17171731, the LA *FAM13B* eQTL SNP, perhaps illuminating heart chamber-specific regulatory variants controlling *FAM13B* gene expression.

**FIGURE 4 FAM13B Localization and Recombinant Protein**

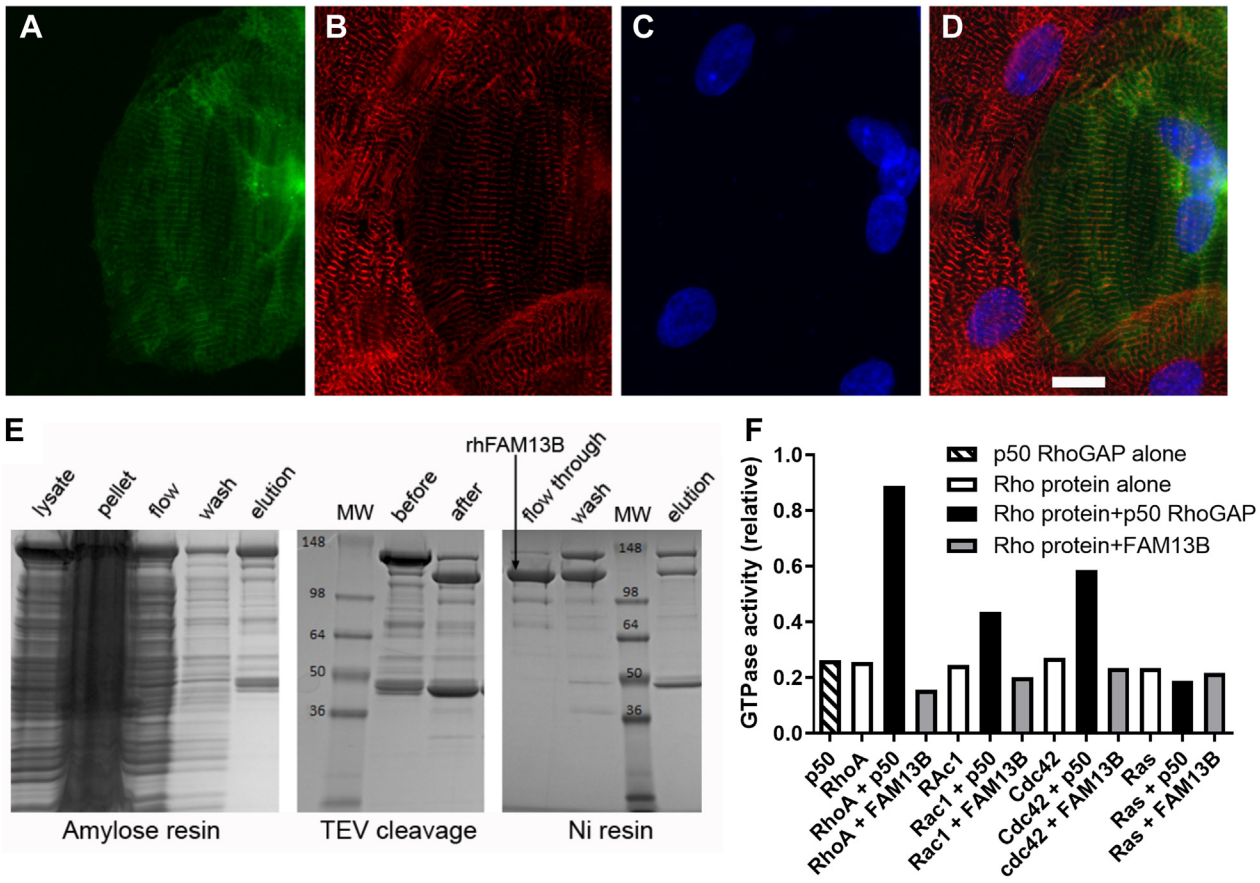


(A–D) FAM13B-GFP fusion protein expression in iCell cardiomyocytes green fluorescent protein (GFP) fluorescence showing expression in a sarcomere pattern and on the plasma membrane (A). (B) α-actinin immunofluorescence (red) showing Z-disc localization with the transfected cell surrounded by nontransfected cells. (C) Hoechst 33342 staining of nuclei. (D) Merged image, showing FAM13B-GFP expression overlaps with or is adjacent to the Z-disc marker protein α-actinin; ×60 objective lens, scale bar shows 20 μm. (E) rhFAM13B purification. 6 Histidine (6xHis)-maltose binding protein (MBP)-hFAM13 fusion protein in bacterial lysate was eluted from an amylose column (left panel), cleaved with 6xHis-Tobacco Etch Virus (TEV) protease releasing the rhFAM13B from the 6xHis-MBP affinity tags (center panel), and purified by flow through in the Ni resin column (right panel). (F) Rho GTPase-activating protein (RhoGAP) activity assay (in singleton assay) showing background GTPase activity of the p50 RhoGAP alone (striped bar) and for each of the 4 Rho proteins alone (white bars), whereas p50 RhoGAP increased the GTPase activity of 3 of 4 Rho proteins (black bars). In contrast, rhFAM13B did not increase GTPase activity for any of the 4 Rho proteins (gray bars).

To begin to assess the functional role of *FAM13B*, we used siRNA KD in human iCell cardiomyocytes, which are pure cardiomyocytes that offer a powerful in vitro model to study novel mechanisms of arrhythmias. RNAseq analysis of the *FAM13B* KD cells showed a striking pattern with extensive coregulation with more than 1,000 other genes, suggesting *FAM13B* may be a hub gene that plays a role in regulating LA physiology. Pathway analysis found a strong empirical network that included *SCN2B*, a subunit of the cardiac sodium channel, which we identified as one of the most downregulated genes. In ventricular cardiomyocytes from normal and heart failure dogs, virally delivered siRNA KD of *SCN2B* was associated with increased late sodium current ($I_{NaL}$),[31] similar to what we observed in human iCell cardiomyocytes after *FAM13B* KD (**Figure 3**). However, sodium currents are not identical in atrial and ventricular cardiomyocytes, likely because of differences in sodium channel subunit composition and cellular architecture.[32] Changes in $I_{NaL}$, resulting from either genetic or environmental influences, have been associated with action potential prolongation in heart failure, and both $I_{NaL}$[33] and mutations in *SCN2B* have been associated with risk of AF.[34] The mouse KO of *Scn2b* also gave subtle differences in the $I_{Na}$.[27] In addition, human iCMs paced for 7 days in an AF-simulated irregular fashion (mean frequency 1 Hz) had

**FIGURE 5** Heart Structure Function and Basal ECG of WT and Fam13b KO mice

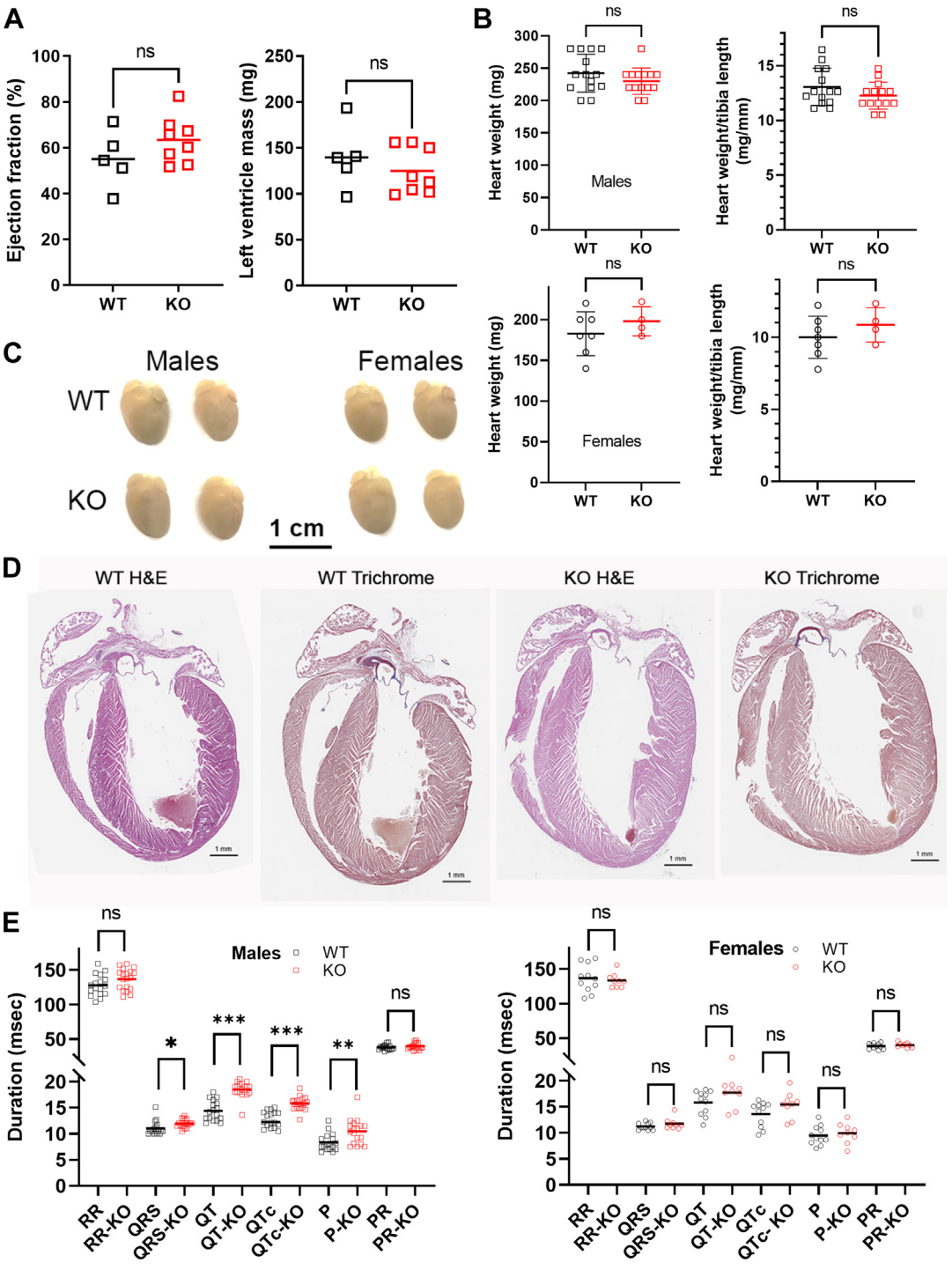


(A) Ejection fraction (left) and left ventricular mass (right) in male wild-type (WT) (n = 5) and knockout (KO) (n = 8) mice (means shown, Student's *t*-test). (B) Heart (left) and heart weight normalized to tibial length (right side) in male (top, 14 WT and 14 KO) and female (bottom, 7 WT and 4 KO) mice (means shown, Student's *t*-test). (C) Gross appearance of representative perfused and fixed hearts ex vivo (Males, left; females, right, WT, top; KO, bottom). (D) Four-chamber fixed section stained with hematoxylin-eosin (H&E) and Masson's Trichrome. (E) Basal electrocardiogram (ECG) readings in male (left, 17 WT and 19 KO) and female (right, 11 WT and 9 KO) WT (black symbols) and KO (red symbols) mice, with each symbol representing a biological replicate. Data were analyzed by Mann-Whitney tests, with median values shown (*$P < 0.05$; **$P < 0.01$; ***$P < 0.001$). P = duration of P-wave; PR = duration of PR interval; QRS = duration of QRS peak; QT = duration of QT interval; QTc = duration of QT interval corrected for a standard heart cycle; RR = duration of heart cycle via RR interval.

**FIGURE 6** **Intracardiac Pacing-Induced Arrhythmia**

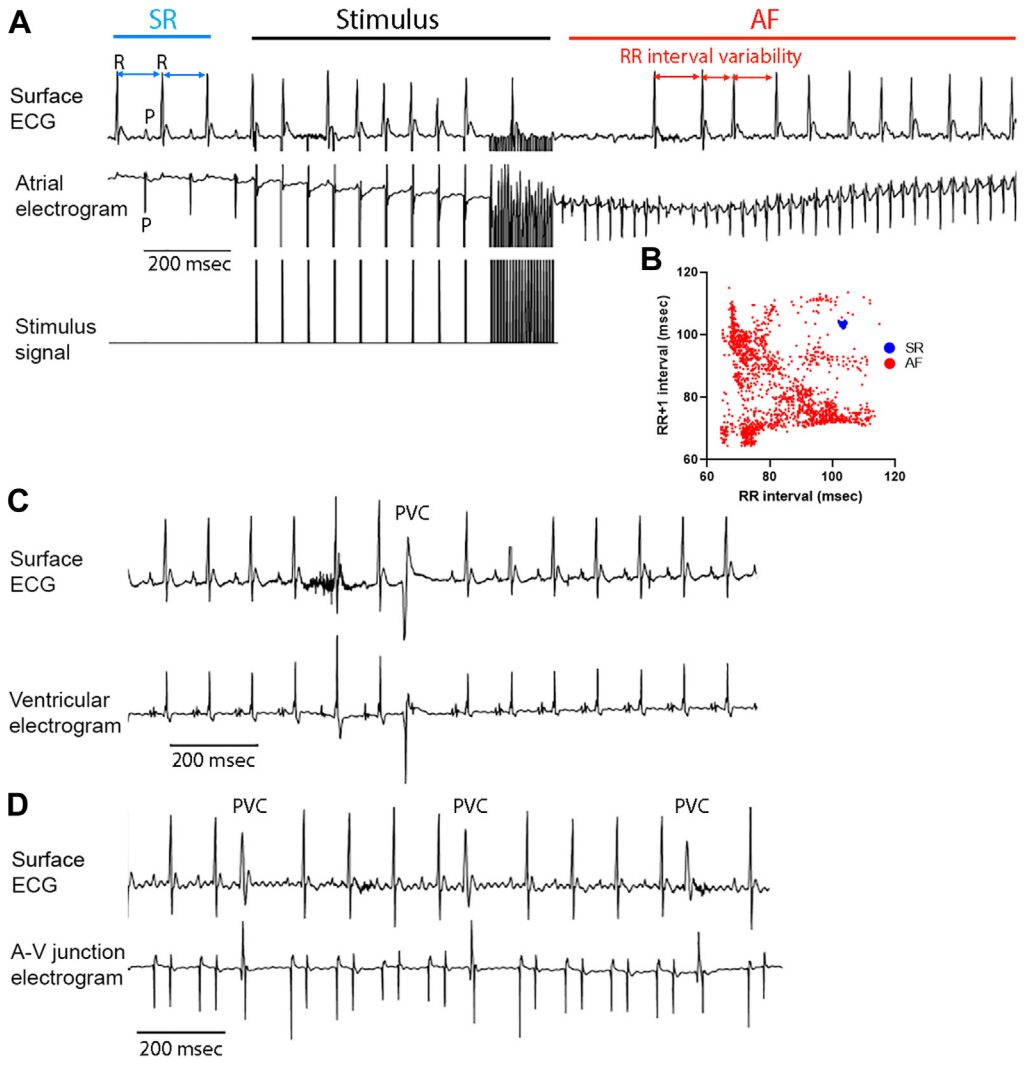


(A) Representative surface electrocardiogram (ECG) and atrial intracardiac electrogram from a female *Fam13b* knockout (KO) mouse showing burst pacing followed by an occurrence of atrial fibrillation (AF) with RR variability and P-wave disruption (SR, sinus rhythm phase with normal P waves and double-headed blue arrows showing the regular RR interval; Stimulus, showing the programmed electrical stimulation; AF, the atrial fibrillation phase with rapid and chaotic atrial activation with lack of regular P waves, the double-headed red arrows showing RR interval variability). AF events stopped spontaneously followed by normal SR. (B) Poincare plot showing representative RR variability in a single female *Fam13b* KO before (black symbols) and after pacing-induced AF (red symbols), with the median RR variability 18 times larger in AF ($P < 0.001$, Mann-Whitney test). (C, D) Representative surface ECGs and intracardiac recordings from 2 male *Fam13b* KO mice showing instances of ventricular arrhythmia due to premature ventricular contractions (PVC).

increased $I_{NaL}$ compared with iCMs regularly paced at 1 Hz, which was accompanied by decreased systolic $Ca^{2+}$ transient amplitude and longer action potential duration, all indicative of a pro-arrhythmia state.[35] Pathway analysis also showed that calcium signaling was the top canonical pathway associated with *FAM13B* KD. Our $Ca^{2+}$ transient study found that *FAM13B* KD led to decreased $Ca^{2+}$ amplitude and slower return to baseline (**Figure 3**), consistent with the pacing-induced pro-arrhythmia state,[35] although we did not measure action potential duration in these studies.

The determinants of peak and late sodium current density are complex, with roles for channel trafficking, CaMKII phosphorylation of SCN5A, subunit interactions, oxidative stress, and metabolic status

**FIGURE 7 Pacing-Induced AF and VA**

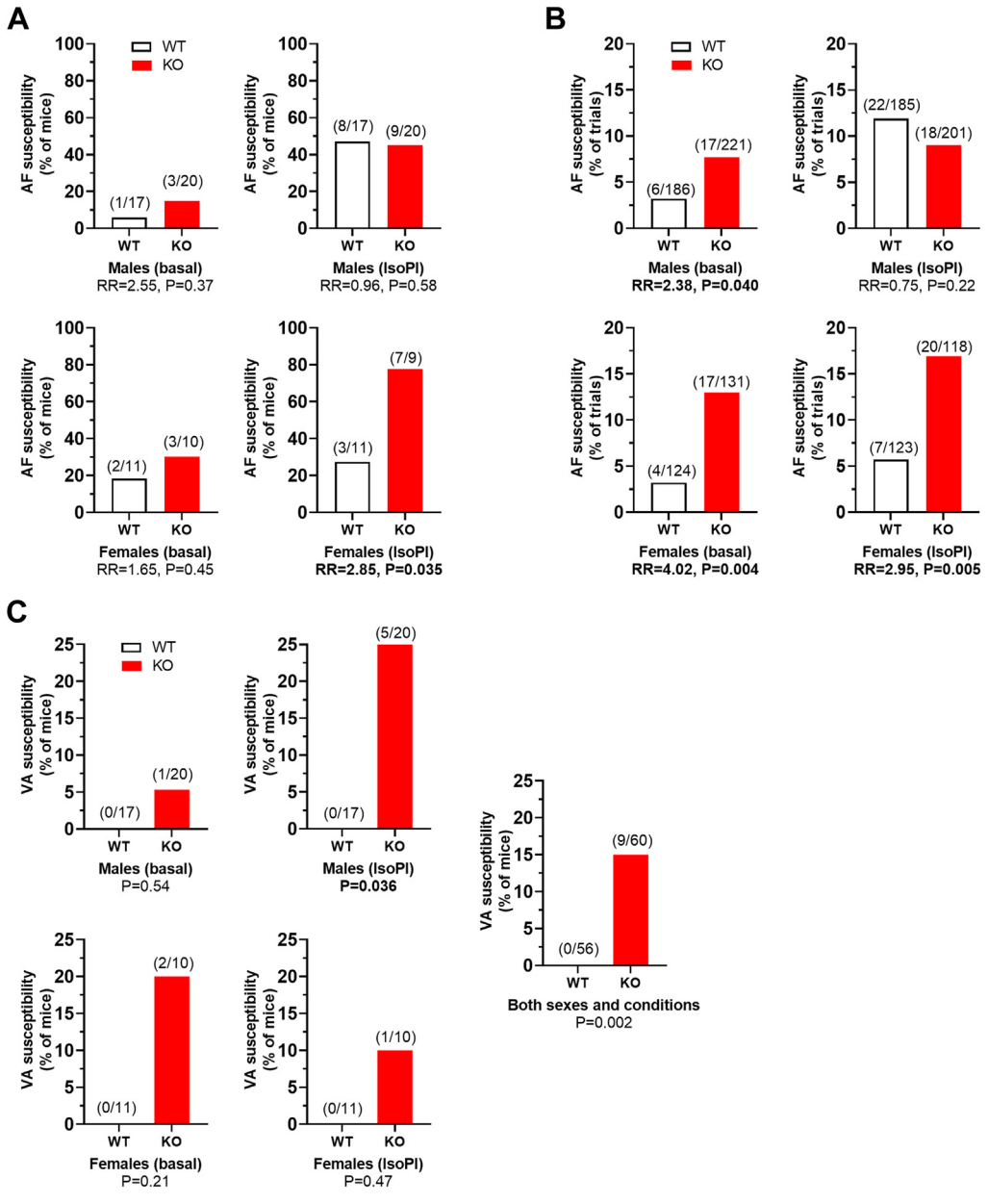


(A) Susceptibility to atrial fibrillation (AF) induction per mouse for male and female wild-type (WT) (white bars) and *Fam13b* knockout (KO) (red bars) mice under basal and isoproterenol (IsoP) conditions. (B) Susceptibility to AF per trial for all mice in each group. (C) Susceptibility to ventricular arrhythmia (VA) per mouse for male and female WT and *Fam13b* KO mice under basal and IsoP conditions, as well as in both sexes and conditions combined. For all plots, (N/N) represents the number in arrhythmia/the total number. The numbers in arrhythmia vs not in arrhythmia were analyzed using Fisher's exact test, with the relative risk (for KO vs WT) and *P* values shown below each graph with *P* values $<0.05$ shown in bold.

suggested as potential modifiers. We suggest that increased $I_{NaL}$, which indirectly modifies intracellular calcium levels as a result of sodium-calcium exchanger activity, may represent one of the pathways whereby a genetically determined reduction in *FAM13B* abundance increases risk of AF. Other sodium channel (eg, *SCN5A*) gain-of-function mutations that increase sodium influx have also been

associated with increased risk of cardiac arrhythmia.[36-38] Our studies suggest that inhibition of $I_{NaL}$ with new or available drugs, such as ranolazine, may reduce AF risk in patients carrying the *FAM13B* risk allele. Although decreased *SCN2B* expression may play a role in the association of low *FAM13B* expression with AF, many other mechanisms are possible, including effects on other ion currents as well as direct effects on sarcomere structure/function.

Expression of a FAM13B-GFP fusion protein in iCell cardiomyocytes demonstrated localization both in sarcomeres and on the plasma membrane (**Figure 4**). The sarcomere staining overlaps or was adjacent to the Z-disc marker protein α-actinin. This pattern may be due to FAM13B localization on the Z-disk and/or the T-tubule, which connects the plasma membrane with deep invaginations near the Z-disk. Using the Gene Ontology list for genes associated with the Z-disk in mice, we found the following other AF GWAS genes[2] that share this association: *CASQ2*, *CFL2*, *FBXO32*, *KCNN2*, *MYH7*, *MYO18B*, *MYOZ1*, *SYNE2*, *SYNPO2L*, and *TTN*.

*FAM13B*, previously known as *C5ORF5*, is in the RhoGAP gene family, but it is predicted to lack RhoGAP catalytic activity due to 2 nonconserved amino acid residues in regions of the protein known to be required for activity.[6] Our recombinant FAM13B protein did not display RhoGAP activity using 4 different Rho proteins; however, it is possible that RhoGAP activity could be present with a different Rho protein. Alternatively, this protein may function as a scaffold or have another unknown catalytic activity.

To determine whether decreased FAM13B expression alters AF susceptibility in vivo, we turned to a KO mouse model. Unlike some other spontaneous AF models with enlarged atria,[39] *Fam13b* KO mice had normal heart size and did not develop spontaneous arrhythmia. However, *Fam13b* KO mice did have changes in their basal ECG with increased P-wave duration and QTc interval, particularly in male mice, demonstrating a potential arrhythmogenic substrate. This is supported by recent population studies that found that P-wave duration and QTc interval are positively associated with AF incidence.[40-45] These studies were looking at QT interval variation in populations, not the variation associated with rare monogenic forms of long QT syndrome. Within the QTc interval, it is the prolonged JT interval rather than the QRS that is associated with AF.[46] However, there was a J-shaped association of QTc with AF, such that those in the fifth percentile or less of QTc were at increased risk of AF; and, those in the 60th or greater percentile of QTc were increasingly at greater risk of AF.[47] The most recent GWAS for JT and QT intervals found highly significant associations, respectively, with rs17171731 ($P = 4E\text{-}23$) and rs1335516 ($P = 1E\text{-}43$, in very high LD with each other in European ancestry populations), with the AF risk allele associated with longer durations.[48] The GTEx project shows relatively low expression of *FAM13B* in human left ventricle (median value 5.5 transcripts per million), and no significant left ventricle *FAM13B* eQTLs are detected. Thus, one cannot determine whether lower *FAM13B* expression in the atria or ventricles leads to prolonged JT and QT intervals. A mendelian randomization study was performed to address whether a longer QT interval is directly causal for AF, and no direct relationship was observed between the polygenic score for QT interval and AF incidence.[49] However, this negative result could be due to genetic heterogeneity, where some QT prolonging alleles promote and others protect from AF.

Our observed increased occurrence of intracardiac pacing-induced AF and ventricular arrhythmia in KO vs WT mice is consistent with the increased pacing-induced AF susceptibility observed for *Scn2b* KO mice.[27] Further implicating the potential role of decreased *SCN2B* expression driving increased $I_{NaL}$ and AF susceptibility downstream of reduced *FAM13B*, a mouse model with an *Scn5a* missense mutation knockin that is resistant to increased $I_{NaL}$ is also resistant to obesity and epinephrine + caffeine-induced atrial arrhythmia.[38,50] Thus, our current studies identified *FAM13B* as the AF modifier gene responsible for the chr5q31 AF locus, consistent with the modest effects on basal ECG and pacing-induced arrhythmia in mice. As a modifier gene, we would not expect to observe the strong in vivo phenotypes that are associated with a monogenic AF gene, such as rare autosomal dominant mutations in the *SCN5A* gene that can lead to long QT syndrome, and/or Brugada syndrome as well as AF.[51,52] Further understanding of the mechanism by which low expression of *FAM13B*, along with its binding partners and associated pathways, can predispose to AF susceptibility may illuminate additional targets for novel therapies. The significant eQTL for *FAM13B* demonstrated in human adult LAA tissues suggest that the *FAM13B* pathway may be a viable therapeutic target in adults with AF, in contrast to the top GWAS locus at 4q25 near PITX2, a transcription factor most active during development.

Although we found effects on sodium current and calcium transients in *FAM13B* KD in iCell cardiomyocytes and on the basal ECG in the global *Fam13b* KO mice, existing human RNAseq data show that *FAM13B* is widely expressed, with the highest

expression in the large arteries (tissue-based) and in vascular smooth muscle cells (LA single-nuclei RNA-seq).[14] We still think that the effects of the AF risk allele are mediated locally in the LA because of our finding that the effect of the eQTL for the top GWAS AF risk SNP rs2040862 (in virtually perfect LD with rs17171731 in European ancestry subjects) is much more significant in the LAA in European ancestry subjects ($P$ = 6.91 E-30) than any other eQTLs for *FAM13B* expression in any other tissue from the GTEx project. The most significant *FAM13B* eQTL in GTEx is for the right atrial appendage, where SNPs in the same LD bin as rs2040862 have $P$ values of ~1.8 E-12. However, the cell type involved in *FAM13B* expression effects on AF susceptibility is not clear. Here we studied the effect of FAM13B KD in iCMs, but additional studies, such as KD in other cell types including vascular smooth muscle cells or the creation of tissue-specific KO mice, will be needed to understand the role of *FAM13B* in the various cell types in the LA.

**STUDY LIMITATIONS.** Although our functional genomics study identified *FAM13B* as the gene responsible for the chr 5q31 AF GWAS locus, and our subsequent cellular studies identified changes in the late sodium current and calcium handling after *FAM13B* knockdown, there are still many unresolved questions pertaining to how does the mRNA expression level of a sarcomeric protein alter the expression levels of so many additional genes, including those genes involved in sodium and calcium trafficking.

## CONCLUSIONS

GWAS identify genetic loci, where common genetic variants are associated with diseases or traits. However, it still takes much effort to identify the responsible gene, the responsible genetic variants, and the mechanism for the trait association. Here, we dissected the AF GWAS locus on chr 5q31. Using our LAA transcriptomic and eQTL studies, especially data from African ancestry subjects, we identified *FAM13B* and rs17171731 as the responsible gene and genetic variant, respectively, where the risk variant is associated with decreased *FAM13B* gene expression. We further demonstrated in cardiomyocytes derived from human stem cells that knockdown of *FAM13B* gene expression altered the expression of many other genes, including those involved in the handling of sodium and calcium ions. Cellular electrophysiology studies confirmed that *FAM13B* knockdown increased the late sodium current and altered calcium handling. Finally, we demonstrated that *Fam13b* knockout mice were more susceptible to intracardiac pacing induced atrial and ventricular arrhythmia, verifying the *FAM13B* gene as an authentic AF risk modifying gene.

## FUNDING SUPPORT AND AUTHOR DISCLOSURES

This work was supported by the National Institutes of Health (NIH) grants RO1 HL 111314 and P01HL158502 to Drs Chung, Van Wagoner, Barnard, and Smith; an American Heart Association Strategically Focused Research Network grant 18SFRN34110067 to Drs Chung, Van Wagoner, Barnard, and Smith; the NIH National Center for Research Resources for Case Western Reserve University and Cleveland Clinic Clinical and Translational Science Award UL1-RR024989; the Cleveland Clinic Department of Cardiovascular Medicine philanthropy research funds; and the Tomsich Atrial Fibrillation Research Fund. Dr Ponce-Balbuena was supported by an American Heart Association Career Development Award 20CDA35320040. Dr Hsu was supported by NIH training grant T32 GM 088088. Dr Smith was supported by the Geoffrey Gund Endowed Chair for Cardiovascular Research. The Fusion Lumos LC-MS instrument was purchased from the NIH shared instrument grant 1S10OD023436. The authors have reported that they have no relationships relevant to the contents of this paper to disclose.

**ADDRESS FOR CORRESPONDENCE:** Dr Mina K. Chung, OR Dr Jonathan D. Smith, Cardiovascular and Metabolic Sciences, Box ND50, Cleveland Clinic, 9500 Euclid Avenue, Cleveland, Ohio 44195, USA. E-mail: chungm@ccf.org OR smithj4@ccf.org.

## PERSPECTIVES

**COMPETENCY IN MEDICAL KNOWLEDGE:** Human genetic association studies for quantitative or qualitative traits provide the lamppost under which scientists can search for the causal genetic variant, the causal gene, the mechanism for the trait association, and confirmation of the association in preclinical models. This functional genomics discovery process illuminates new genes and pathways in human pathophysiology and thus may have large implications for the development of new and targeted therapeutics to prevent and treat diseases.

**TRANSLATIONAL OUTLOOK:** Here we describe *FAM13B* as a new gene with a protective role against atrial fibrillation susceptibility. This work adds to our knowledge base on structural sarcomeric proteins that can affect cellular electrophysiology and arrhythmogenesis. Future studies may attempt to counteract the effects of decreased *FAM13B* expression by finding drugs that target the genes and pathways altered by *FAM13B* knockdown.

## REFERENCES

**1.** Ellinor PT, Yoerger DM, Ruskin JN, MacRae CA. Familial aggregation in lone atrial fibrillation. *Hum Genet*. 2005;118:179–184.

**2.** Roselli C, Chaffin MD, Weng LC, et al. Multi-ethnic genome-wide association study for atrial fibrillation. *Nat Genet*. 2018;50:1225–1233.

**3.** Nielsen JB, Thorolfsdottir RB, Fritsche LG, et al. Biobank-driven genomic discovery yields new insight into atrial fibrillation biology. *Nat Genet*. 2018;50:1234–1239.

**4.** Choi SH, Jurgens SJ, Weng LC, et al. Monogenic and polygenic contributions to atrial fibrillation risk: results from a national biobank. *Circ Res*. 2020;126:200–209.

**5.** Hsu J, Gore-Panter S, Tchou G, et al. Genetic control of left atrial gene expression yields insights into the genetic susceptibility for atrial fibrillation. *Circ Genom Precis Med*. 2018;11:e002107.

**6.** Lai F, Godley LA, Fernald AA, et al. cDNA cloning and genomic structure of three genes localized to human chromosome band 5q31 encoding potential nuclear proteins. *Genomics*. 2000;70:123–130.

**7.** Cohen M, Reichenstein M, Everts-van der Wind A, et al. Cloning and characterization of FAM13A1–a gene near a milk protein QTL on BTA6: evidence for population-wide linkage disequilibrium in Israeli Holsteins. *Genomics*. 2004;84:374–383.

**8.** Human LAA eQTL data. Accessed October 4, 2023. https://afeqtls.lerner.ccf.org/

**9.** Custom Scripts for eQTL analyses. Accessed October 4, 2023. https://github.com/jeffhsu3/genda

**10.** Dryad Accession Number. Accessed October 4, 2023. https://doi.org/10.5061/dryad.nk98sf7xj

**11.** Marchini J, Howie B, Myers S, McVean G, Donnelly P. A new multipoint method for genome-wide association studies by imputation of genotypes. *Nat Genet*. 2007;39:906–913.

**12.** Shabalin AA. Matrix eQTL: ultra fast eQTL analysis via large matrix operations. *Bioinformatics*. 2012;28:1353–1358.

**13.** Storey JD, Tibshirani R. Statistical significance for genomewide studies. *Proc Natl Acad Sci U S A*. 2003;100:9440–9445.

**14.** Tucker NR, Chaffin M, Fleming SJ, et al. Transcriptional and cellular diversity of the human heart. *Circulation*. 2020;142:466–482.

**15.** Hao Y, Hao S, Andersen-Nissen E, et al. Integrated analysis of multimodal single-cell data. *Cell*. 2021;184:3573–3587.e29.

**16.** Stuart T, Butler A, Hoffman P, et al. Comprehensive integration of single-cell data. *Cell*. 2019;177:1888–1902.e21.

**17.** McCarthy DJ, Chen Y, Smyth GK. Differential expression analysis of multifactor RNA-Seq experiments with respect to biological variation. *Nucleic Acids Res*. 2012;40:4288–4297.

**18.** Nordeen SK. Luciferase reporter gene vectors for analysis of promoters and enhancers. *Biotechniques*. 1988;6:454–458.

**19.** Law CW, Chen Y, Shi W, Smyth GK. voom: precision weights unlock linear model analysis tools for RNA-seq read counts. *Genome Biol*. 2014;15:R29.

**20.** Giner G, Smyth GK. FRY: a fast approximation to ROAST gene set test with mean aggregated set statistics. *F1000Research*. 2016;5:2605 (slides).

**21.** Ritchey B, Hai Q, Han J, Barnard J, Smith JD. Genetic variant in 3′ untranslated region of the mouse pycard gene regulates inflammasome activity. *Elife*. 2021;10:e68203.

**22.** Conant D, Hsiau T, Rossi N, et al. Inference of CRISPR edits from Sanger trace data. *CRISPR J*. 2022;5:123–130.

**23.** Valli H, Ahmad S, Fraser JA, Jeevaratnam K, Huang CL. Pro-arrhythmic atrial phenotypes in incrementally paced murine Pgc1β(-/-) hearts: effects of age. *Exp Physiol*. 2017;102:1619–1634.

**24.** Vasudevan NT, Mohan ML, Gupta MK, et al. Gβγ-independent recruitment of G-protein coupled receptor kinase 2 drives tumor necrosis factor alpha-induced cardiac beta-adrenergic receptor dysfunction. *Circulation*. 2013;128:377–387.

**25.** Filgueiras-Rama D, Vasilijevic J, Jalife J, et al. Human influenza A virus causes myocardial and cardiac-specific conduction system infections associated with early inflammation and premature death. *Cardiovasc Res*. 2021;117:876–889.

**26.** Li N, Wehrens XH. Programmed electrical stimulation in mice. *J Vis Exp*. 2010;39:1730.

**27.** Bao Y, Willis BC, Frasier CR, et al. Scn2b deletion in mice results in ventricular and atrial arrhythmias. *Circ Arrhythm Electrophysiol*. 2016;9:e003923.

**28.** Mathelier A, Fornes O, Arenillas DJ, et al. JASPAR. 2016: a major expansion and update of the open-access database of transcription factor binding profiles. *Nucleic Acids Res*. 2016;44:D110–D115.

**29.** Meng X, Nie Y, Wang K, Fan C, Zhao J, Yuan Y. Identification of atrial fibrillation-associated genes ERBB2 and MYPN using genome-wide association and transcriptome expression profile data on left-right atrial appendages. *Front Genet*. 2021;12:696591.

**30.** Arking DE, Pulit SL, Crotti L, et al. Genetic association study of QT interval highlights role for calcium signaling pathways in myocardial repolarization. *Nat Genet*. 2014;46:826–836.

**31.** Mishra S, Undrovinas NA, Maltsev VA, Reznikov V, Sabbah HN, Undrovinas A. Post-transcriptional silencing of SCN1B and SCN2B genes modulates late sodium current in cardiac myocytes from normal dogs and dogs with chronic heart failure. *Am J Physiol Heart Circ Physiol*. 2011;301:H1596–H1605.

**32.** Luo A, Ma J, Song Y, et al. Larger late sodium current density as well as greater sensitivities to ATX II and ranolazine in rabbit left atrial than left ventricular myocytes. *Am J Physiol Heart Circ Physiol*. 2014;306:H455–H461.

**33.** Fischer TH, Herting J, Mason FE, et al. Late INa increases diastolic SR-Ca2+-leak in atrial myocardium by activating PKA and CaMKII. *Cardiovasc Res*. 2015;107:184–196.

**34.** Watanabe H, Darbar D, Kaiser DW, et al. Mutations in sodium channel beta1- and beta2-subunits associated with atrial fibrillation. *Circ Arrhythm Electrophysiol*. 2009;2:268–275.

**35.** Pabel S, Knierim M, Stehle T, et al. Effects of atrial fibrillation on the human ventricle. *Circ Res*. 2022;130:994–1010.

**36.** Tian XL, Yong SL, Wan X, et al. Mechanisms by which SCN5A mutation N1325S causes cardiac arrhythmias and sudden death in vivo. *Cardiovasc Res*. 2004;61:256–267.

**37.** Blana A, Kaese S, Fortmuller L, et al. Knock-in gain-of-function sodium channel mutation prolongs atrial action potentials and alters atrial vulnerability. *Heart Rhythm*. 2010;7:1862–1869.

**38.** Glynn P, Musa H, Wu X, et al. Voltage-gated sodium channel phosphorylation at Ser571 regulates late current, arrhythmia, and cardiac function in vivo. *Circulation*. 2015;132:567–577.

**39.** Fu F, Pietropaolo M, Cui L, et al. Lack of authentic atrial fibrillation in commonly used murine atrial fibrillation models. *PLoS One*. 2022;17:e0256512.

**40.** Khurshid S, Friedman S, Reeder C, et al. ECG-based deep learning and clinical risk factors to predict atrial fibrillation. *Circulation*. 2022;145:122–133.

**41.** Xie E, Wu C, Ostovaneh M, et al. Intermediate markers underlying electrocardiographic predictors of incident atrial fibrillation: the MESA. *Circ Arrhythm Electrophysiol*. 2021;14:e009805.

**42.** Nguyen KT, Vittinghoff E, Dewland TA, et al. Electrocardiographic predictors of incident atrial fibrillation. *Am J Cardiol*. 2016;118:714–719.

**43.** Radnahad N, Ehrlinder H, Leander K, Engdahl J, Wallen H, Gigante B. Is the association of QTc with atrial fibrillation and stroke in cohort studies a matter of time? *Open Heart*. 2022;9:e002080.

**44.** Mandyam MC, Soliman EZ, Alonso A, et al. The QT interval and risk of incident atrial fibrillation. *Heart Rhythm*. 2013;10:1562–1568.

**45.** O'Neal WT, Efird JT, Kamel H, et al. The association of the QT interval with atrial fibrillation and stroke: the Multi-Ethnic Study of Atherosclerosis. *Clin Res Cardiol*. 2015;104:743–750.

**46.** Patel N, O'Neal WT, Whalen SP, Soliman EZ. The association of QT interval components with atrial fibrillation. *Ann Noninvasive Electrocardiol*. 2018;23:e12467.

**47.** Nielsen JB, Graff C, Pietersen A, et al. J-shaped association between QTc interval duration and the risk of atrial fibrillation: results from the Copenhagen ECG study. *J Am Coll Cardiol*. 2013;61:2557–2564.

**48.** Young WJ, Lahrouchi N, Isaacs A, et al. Genetic analyses of the electrocardiographic QT interval and its components identify additional loci and pathways. *Nat Commun*. 2022;13:5144.

**49.** Gajendragadkar PR, Von Ende A, Ibrahim M, et al. Assessment of the causal relevance of ECG parameters for risk of atrial fibrillation: a mendelian randomisation study. *PLoS Med*. 2021;18:e1003572.

**50.** Dewal RS, Greer-Short A, Lane C, et al. Phospho-ablation of cardiac sodium channel Nav1.5 mitigates susceptibility to atrial fibrillation and improves glucose homeostasis under conditions of diet-induced obesity. *Int J Obes*. 2021;45:795–807.

**51.** Darbar D, Kannankeril PJ, Donahue BS, et al. Cardiac sodium channel (SCN5A) variants associated with atrial fibrillation. *Circulation*. 2008;117:1927–1935.

**52.** Wan E, Abrams J, Weinberg RL, et al. Aberrant sodium influx causes cardiomyopathy and atrial fibrillation in mice. *J Clin Invest*. 2016;126:112–122.

**KEY WORDS** CRISPR gene editing, functional genomics, pacing-induced arrhythmia, Rho GTPase-activating protein

**APPENDIX** For supplemental tables and figures, please see the online version of this paper.